INTERNATIONAL JOURNAL OF HYDROGEN ENERGY 40 (2015) 10308–10328

Available online at www.sciencedirect.com

ScienceDirect

journal homepage: www.elsevier.com/locate/he

Influence of fuel hydrogen fraction on syngas fueled SI engine: Fuel thermo-physical property analysis and in-cylinder experimental investigations

Anand M. Shivapuji [1], *S. Dasappa* [*]

Center for Sustainable Technologies, Indian Institute of Science, Bangalore 560012, India

ARTICLE INFO

Article history:
Received 20 March 2015
Received in revised form
11 June 2015
Accepted 12 June 2015
Available online 9 July 2015

Keywords:
Syngas
Hydrogen
Conductivity
Diffusivity
Convective cooling

ABSTRACT

Hydrogen, either in pure form or as a gaseous fuel mixture specie enhances the fuel conversion efficiency and reduce emissions in an internal combustion engine. This is due to the reduction in combustion duration attributed to higher laminar flame speeds. Hydrogen is also expected to increase the engine convective heat flux, attributed (directly or indirectly) to parameters like higher adiabatic flame temperature, laminar flame speed, thermal conductivity and diffusivity and lower flame quenching distance. These factors (adversely) affect the thermo-kinematic response and offset some of the benefits.

The current work addresses the influence of mixture hydrogen fraction in syngas on the engine energy balance and the thermo-kinematic response for close to stoichiometric operating conditions. Four different bio-derived syngas compositions with fuel calorific value varying from 3.14 MJ/kg to 7.55 MJ/kg and air fuel mixture hydrogen fraction varying from 7.1% to 14.2% by volume are used. The analysis comprises of (a) use of chemical kinetics simulation package CHEMKIN for quantifying the thermo-physical properties (b) 0-D model for engine in-cylinder analysis and (c) in-cylinder investigations on a two-cylinder engine in open loop cooling mode for quantifying the thermo-kinematic response and engine energy balance.

With lower adiabatic flame temperature for Syngas, the in-cylinder heat transfer analysis suggests that temperature has little effect in terms of increasing the heat flux. For typical engine like conditions (700 K and 25 bar at CR of 10), the laminar flame speed for syngas exceeds that of methane (55.5 cm/s) beyond mixture hydrogen fraction of 11% and is attributed to the increase in H based radicals. This leads to a reduction in the effective Lewis number and laminar flame thickness, potentially inducing flame instability and cellularity.

Use of a thermodynamic model to assess the isolated influence of thermal conductivity and diffusivity on heat flux suggests an increase in the peak heat flux between 2% and 15% for the lowest (0.420 MW/m^2) and highest (0.480 MW/m^2) hydrogen containing syngas over methane (0.415 MW/m^2) fueled operation. Experimental investigations indicate the engine cooling load for syngas fueled engine is higher by about 7% and 12% as compared to methane fueled operation; the losses are seen to increase with increasing mixture hydrogen fraction. Increase in the gas to electricity efficiency is observed from 18% to 24%

* *Corresponding author*. Tel.: +91 9845598203.
E-mail address: dasappa@cgpl.iisc.ernet.in (S. Dasappa).
[1] Tel.: +91 9448775050.

http://dx.doi.org/10.1016/j.ijhydene.2015.06.062

as the mixture hydrogen fraction increases from 7.1% to 9.5%. Further increase in mixture hydrogen fraction to 14.2% results in the reduction of efficiency to 23%; argued due to the changes in the initial and terminal stages of combustion. On doubling of mixture hydrogen fraction, the flame kernel development and fast burn phase duration decrease by about 7% and 10% respectively and the terminal combustion duration, corresponding to 90%–98% mass burn, increases by about 23%. This increase in combustion duration arises from the cooling of the near wall mixture in the boundary layer attributed to the presence of hydrogen. The enhancement in engine cooling load and subsequent reduction in the brake thermal efficiency with increasing hydrogen fraction is evident from the engine energy balance along with the cumulative heat release profiles.

Introduction

The primary focus of global research in the field of internal combustion (IC) engines is towards maximizing thermal efficiency and minimizing carbon emissions. Hydrogen as a fuel source, can potentially meet both the objectives. Being a zero carbon fuel, H_2 combustion generates carbon free exhaust. With higher laminar flame speed/adiabatic flame temperature compared to other fuels (refer Table 1) engines fueled with H_2 are expected to have superior thermal efficiency. Towards this, research is being directed at fuelling spark ignited (SI) engines with H_2/H_2 containing mixtures (combustible compounds with H_2 as a constituent) [1–5], the latter being the preferred choice considering the challenges associated with direct H_2 fueled operation like pre-ignition, inlet manifold backfire [4,6], high pressure rise rates [5,7] and NO_x formation [8,9] etc. The basic philosophy is to blend H_2 with other fuels to improve the combustion characteristics, specifically to extend/improve the lean limit operation [9–11] and as a fuel specie as in syngas [12–15]. The use of H_2 with CH_4 (designated hythane), especially under lean operating conditions, is one of the key areas begin exhaustively explored under this philosophy [16–18].

While fuelling engines with H_2 containing mixtures may seem well aligned to satisfy the mandatory requirement of curtailing carbon emissions, either directly through fuel substitution or indirectly by efficiency improvement, analysis of the thermo-physical properties of H_2 containing mixtures suggest challenges towards realization of some of the envisaged benefits. Interestingly, the same thermo-physical characteristics of H_2 that support combustion characteristics also tend to pose challenges in realizing the benefits, especially in the close to stoichiometric operation regime.

Table 1 – Thermo-physical properties of hydrogen and other fuels.

	Hydrogen H_2	Gasoline C_8H_{18}	Methane CH_4
Stoichiometric A/F (kg/kg)	34.20	17.19	15.08
Flammability limit (ϕ) [1,2]	0.1–7.1	0.7–4.0	0.5–1.67
Lower heating value (MJ/kg) [19]	119.93	44.50	50.02
Minimum ignition energy (mJ) [1,2]	0.02	0.28	0.24
Density (NTP conditions) (kg/m^3)	0.0831	4.4	0.665
Carbon to Hydrogen ratio (mol/mol)	0.0	0.44	0.25
Laminar flame speed (m/s) [19,20]	265–325	37–43	37–45
Adiabatic flame temperature (K) [19]	2318	2470	2148
Flame quenching distance (cm) [19,20]	0.064	0.20	0.20
Thermal conductivity (W/mK) [3]	0.182	0.011	0.034
Diffusion coefficient (cm^2/s) [3,20]	0.61	0.05	0.16

Numbers in square brackets indicate references for the respective properties.

The challenges

Certain key thermo-physical properties of H_2 containing mixtures that directly and indirectly enhance the engine efficiency also increase the engine cooling load, potentially offsetting the benefits sought to be derived. The laminar flame speed, adiabatic flame temperature, mixture thermal conductivity/diffusivity (all of which increase with H_2 fraction) and flame quenching distance (which decreases with H_2 fraction) are some of the key thermo-physical properties that potentially have dual influence. While higher laminar flame speed and adiabatic flame temperature influence both the efficiency and heat transfer, the flame quenching distance and mixture thermal conductivity/diffusivity directly influence the convective heat transfer between the working fluid and the containing surface(s). The relevant thermophysical properties of H_2, gasoline and CH_4 are consolidated for comparison in Table 1. While the effect of laminar flame speed and adiabatic flame temperature on the thermal efficiency is well established [9,21,22], the influence of described parameters on engine heat transfer is briefly described as below.

1. *Flame speed*: Hydrogen increases the mixture laminar (and hence turbulent) flame speed [23,24], leading to shorter

combustion duration and a greater degree of constant volume combustion. Reduced combustion duration causes higher in-cylinder temperature (high heat release rate) thereby higher temperature gradient, enhancing the heat flux across the wall. Higher flame speeds further enhance the convective heat flux by increasing the fluid turbulence just ahead of the propagating front.

2. *Adiabatic flame temperature*: The adiabatic flame temperature of H_2 is significantly higher as compared to other fuels, leading to higher in-cylinder temperature and temperature gradients, enhancing the wall heat flux.
3. *Flame quenching distance*: Flames with H_2 mixtures have a smaller quenching distance compared to their corresponding hydrocarbon flames. A smaller quenching distance means the flame front is positioned closer to the wall. This increases the spatial temperature gradient and enhances the fluid motion between the flame front and the wall (flame front driven charge motion) consequentially enhancing the heat flux.
4. *Thermal conductivity and diffusivity*: Higher thermal conductivity/diffusivity enhances the engine heat flux through enhanced convective heat transfer coefficient, especially from the un-burned segment of the in-cylinder gases.

It is evident from the foregone discussion that the presence of H_2 in the working fluid has the potential to enhance convective heat loss from the engine. The increase in convective heat flux unfavorably skews the energy balance and negatively influences the engine power rating and emissions. This is evident from the analysis of the engine power rating expression as in equation (1). For a given set of engine parameters (like speed and swept volume), the peak supported load by an engine frame is primarily governed by the fuel thermo-physical properties and the brake thermal efficiency. While the influence of density and calorific value are explicit (refer Table 1), the concern sought to be addressed in the current investigation pertains to the influence of the identified parameters on the brake thermal efficiency and consequently on the power rating and emissions.

$$P = \underbrace{\left[\eta_v * V_s * \frac{N}{60n}\right]}_{\text{Engine parameters}} * \underbrace{[\rho_{mix-a} * Q_{mix-lcv}]}_{\text{Thermophysical properties}} * \eta_t \quad (1)$$

η_t	Thermal efficiency
η_v	Volumetric efficiency
ρ_{mix-a}	Mixture density
N	Engine speed
P	Power
$Q_{mix-lcv}$	Mixture calorific value
V_s	Swept volume
CR	Compression ratio
IC	Internal combustion
MBT	Maximum brake torque
NG	Natural gas
PG	Producer gas
SI	Spark ignited
TDC	Top dead center

Earlier studies

The previous discussion suggests potential enhanced cooling load on fuelling engines with H_2 containing mixtures. Documented operational experience with producer gas (PG), a bio-derived gaseous fuel with composition of about 20% H_2 and CO, 2% CH_4, 12% CO_2 and balance N_2 [25] confirms the same. In the operation of a six-cylinder natural gas (NG) engine fueled with PG, the authors observed enhanced cooling load by about 5.5 ± 0.5% compared to typical values for conventional fuels [26–28]. Similar observations have also been made by Sridhar [29] in operating an SI engine with PG over a range of compression ratios (CR) on a three cylinder engine of different geometric configuration. A consequential drop in the fuel conversion efficiency was also observed. The observations were corroborated by comparing the wide open throttle maximum brake torque (MBT) apparent heat release profiles for PG and NG fulled operation as in Fig. 1. The combustion duration for PG fueled operation, especially the second half, is significantly larger than the corresponding NG combustion duration, suggesting slow burning of the mixture. With PG having higher reference burning velocity as compared to NG, the increase in combustion duration can only be attributed to the reduced flame speed due to cooling of the mixture [24]. The interpretation is further corroborated by the fact that the exhaust gas temperature for PG fueled operation was about 75 K higher as compared to NG exhaust gas temperature [26,29,30] (higher exhaust gas temperature is indicative of late burning [21]). The inset data in Fig. 1 qualifies some of the observations.

Review of literature

Limited literature is available addressing H_2/H_2 containing mixtures fueled engine operation with reference to the influence on engine cooling load. The key findings of the available literature are consolidated as below.

Shudo et al. [31,32] have compared the wall heat flux for engine operation with CH_4 and H_2. For stoichiometric engine operation at fixed volumetric efficiency and MBT ignition timing (corresponding to each fuel) Shudo et al. report the heat flux for H_2 fueled engine operation to be 7 ± 0.5 J/m^2–degCA as compared to 4.5 ± 0.5 J/m^2–degCA for CH_4 fueled operation.

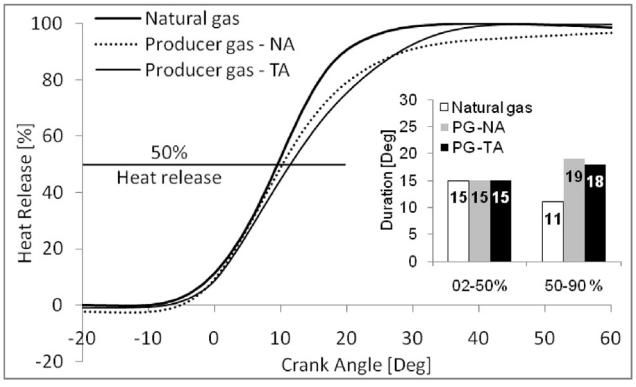

Fig. 1 – Heat release profile and duration for producer gas and natural gas.

Further, in a spark sweep test covering 45° before the top dead center (TDC) to 9° before the TDC for CH_4 and 18° before the TDC to 18° after the TDC for H_2, it was observed that the peak heat flux with H_2 as the fuel was 8 J/m^2–degCA (72 kW/m^2 at 1500 rpm) higher than that for CH_4 fueled engine operation. The increase in convective flux for H_2 fueled operation is explicitly evident. Having established higher heat loss from H_2 fueled engines as compared to CH_4 fueled engines, Shudo et al. have explored options to curtail the convective losses and have suggested stratified charge injection [33] as one of the most optimal strategies. In stratified charge injection a lean but ignitable H_2–air mixture is inhaled by the engine during the suction stroke and is compressed. Subsequently, H_2 is injected, mostly into the adiabatic core, just before ignition to raise the overall stoichiometry to the desired levels. This broadly isolates the H_2 dominant region from the convective heat transfer regime. Adopting this strategy, close to 15% reduction in cooling load has been observed. Extending the analysis to simulation studies, Shudo et al. have suggested that the heat flux in the case of H_2 fueled operation cannot be accurately estimated using conventional heat transfer coefficients (like Annand's, Woschni's etc) and have proposed a new convective heat transfer correlation [34]. Similarly, Demuynck et al. [35], based on wall temperature and flux measurement establish that conventional coefficients are not suitable for capturing convective heat transfer for H_2 and H_2 containing fuels. Along similar lines, Ma et al. [9] have observed an increase in the cooling load as H_2 fraction in H_2–CNG blend increased. It is reported that the ratio of engine cooling load to the cycle energy input increases from around 23% for pure CH_4 operation to about 26% for hythane operation with 50% hydrogen fraction by volume, leading to a reduction in the stoichiometric operation brake thermal efficiency by about 2% points. Knop et al. [36] highlight the need for adopting various sub modules particularly the heat transfer and heat release module when H_2 appears as a fuel component in engines.

Scope and approach of the current work

Analysis of the thermo-physical properties, operational experience with PG as a fuel and review of literature clearly suggest an increase in the heat loss from the engine with subsequent influence on the overall engine performance. While the authors own experience with PG and the work by Shudo et al. attempts to quantify the heat loss, detailed corroborative evidence based on engine energy balance and heat release profile over a range of H_2 fractions is virtually non existent in combustion literature. Towards bridging this gap, the current work addresses the influence of H_2 fraction in syngas on the performance of an NG engine fueled with syngas. In addressing the influence of syngas H_2 fraction on the engine performance, the explicit focus is on;

1. identifying the key thermo-physical properties of syngas/syngas–air mixture that explicitly influence the engine performance and address their sensitivity to syngas H_2 fraction using the chemical kinetics package CHEMKIN [37].
2. using the identified properties in a thermodynamic engine simulation model to quantify their consolidated influence.
3. operating an engine with different syngas compositions, varying in mixture H_2 fraction, in open loop engine cooling mode to quantify the influence of mixture H_2 fraction on the wall heat flux.
4. acquisition and analysis of in-cylinder pressure and heat release profile(s) to quantify the influence of mixture H_2 fraction on in-cylinder apparent heat release and thermo-kinematic response. Special emphasis is on discretizing the heat release profile towards analyzing the influence of mixture H_2 fraction.

While points 3 and 4 explicitly establish and quantify the influence of mixture H_2 fraction on the energy balance, point 1 and 2 provide the scientific justification for the observed behavior. The authors believe that the current study is critical considering that significant emphasis is on fuelling engines with syngas and/or using H_2 as an additive to improve the combustion characteristics.

Materials and methods

The influence of H_2 fraction in syngas on engine performance is addressed through numerical simulations and parametric investigation (including in-cylinder pressure trace acquisition) on a two cylinder four stroke SI engine fueled with four different syngas compositions. The details pertaining to syngas generation, gas composition, engine and instrumentation specification along with the experimental and numerical investigation methodology are presented in the following subsections.

Syngas: generation and composition

Syngas gas used in the current investigation is generated in-situ from a down-draft gasifier that can be operated with air or oxy-steam mixture as the gasifying agent depending on the syngas composition required. Gasification of biomass with air as the gasifying agent generally results in syngas with typical composition of 20% CO and H_2, 2% CH_4, 12% CO_2 and balance 46% N_2. Replacing air with a mixture of oxygen and steam (Oxy-steam) as the gasifying agent effectively eliminating the inerts (N_2) while introducing additional source of H_2 (steam) resulting in an enhancement in the fraction of combustible components. The required H_2 to CO ratio in the syngas can be achieved by controlling the steam to biomass ratio. Using air and oxy-steam gasification, four different syngas compositions, designated C1 to C4, as listed in Table 2 are generated. The reader is referred to Dasappa et al. [25,38] for further details including construction and operation of air gasification system and Sandeep and Dasappa for Oxy-Steam gasification [39,40].

Assessment of data consolidated in Table 2 indicates a general increase in combustibles fraction, with H_2 experiencing close to threefold increase. However, analysis of the mixture composition, which is more relevant from an engine perspective indicates that, while CO and CH_4 fractions in the mixture remain almost invariant, a near two fold increase in

Table 2 – Syngas and stoichiometric mixture composition in volume %.

Designation	CO	H_2	CH_4	CO_2	N_2	O_2
Fuel gas (%)						
C1	11.5	12.8	02.3	10.8	62.6	00.0
C2	13.0	19.4	02.8	11.3	53.5	00.0
C3	14.4	25.9	02.9	19.0	37.8	00.0
C4	16.4	37.2	03.6	24.7	18.1	00.0
Stoichiometric mixture (%)						
C1	06.4	07.1	01.3	06.0	69.9	09.3
C2	06.4	09.5	01.4	05.5	66.5	10.7
C3	06.4	11.6	01.3	08.5	60.6	11.6
C4	06.3	14.2	01.4	09.4	55.7	13.0

the H_2 fraction is observed. As such, performance variations, if any, on fuelling the engine with the four different compositions can broadly be attributed to variation in H_2 fraction.

Investigation methodology

Experimental investigations towards addressing the influence of syngas composition on the engine performance were carried out in two stages. The first stage involved the identification of MBT ignition timing and the corresponding peak load for the four gas compositions. The engine operation was characterized at the respective peak load at MBT, representing the wide open throttle condition. The second stage involved engine operation and characterization at respective MBT timing and at a fixed load (the least of peak loads of the four different gas compositions has been chosen). The peak and common load operation correspond and cater to two different baseline scenarios. The choice of the mixture quality is primarily based on review of literature which suggests that for various H_2 containing gases the brake thermal efficiency peaks at mixture quality around $\phi = 0.85$ [9,19,41,42]. Thus, with mixture quality of $\phi = 0.85$, the engine performance corresponding to maximum brake thermal efficiency was sought to be quantified.

For both peak and part load operation, the air and gas flow rates, engine cooling jacket water flow rate along with the inlet and exit temperature (to quantify cooling load) and in-cylinder pressure traces for 250 consecutive cycles are acquired.

Engine and instrumentation specification

The engine used in the current investigation is a NG engine derived from a diesel frame. The baseline diesel and SI operation specifications of the engine are as listed in Table 3. The engine, rated at 15 kWe under diesel mode is expected to deliver about 7.8 kWe under standard composition PG (20% CO and H_2, 2% CH_4, 12% CO_2 and balance 46% N_2) fueled operation. This assessment is based on previous experience with PG fueled operation wherein it has been observed that under naturally aspirated and stoichiometric operation, the peak load delivered by the engine is limited to about 4.65 kWe per litre of swept volume. The factors contributing to power derating and the corresponding recovery options have been discussed by Dasappa [43] and the authors [27] elsewhere.

Table 3 – Specifications of the engine.

Cylinders	2
Bore/Stroke/Displacement	91.44 (mm)/127 (mm)/1.67 (L)
Aspiration	Natural
Engine speed	1500 rpm
Cooling	Water cooled
Specific to diesel mode	
Compression ratio	18.5:1
Rated output	15 kWe
Specific to gas mode	
Compression ratio	11.0:1
Expected output with PG[a]	about 7.8 kWe at $\phi = 1$

[a] For composition of 20% CO and H_2 and 2% CH_4, balance incombustibles.

The in-cylinder pressure is measured using an AVL make spark plug adapted, un-cooled, piezo-electric, differential pressure sensor (GH13Z) at an acquisition frequency of 90 kHz. Differential to absolute conversion is by using a manifold pressure sensor with a reference pressure supplement. Data is acquired using an eight channel acquisition module (AVL IndiModul) while real time processing and display is by means of a graphical user interface (AVL IndiCom). The electrical power delivered by the engine is measured using a Watt meter while the temperature and flow measurement is through thermocouples and venturi-manometer assembly respectively. Fuel and flue gas composition are measured using SICK MAIHAK and KANE QUINTOX gas analyzers. The range and accuracy of the instruments used in the current analysis are listed in Table 4 below.

Syngas thermo-physical properties

The chemical to mechanical energy conversion in an SI engine, through phased heat release in the combustion chamber, is significantly influenced by the mixture thermo-physical properties. As such, to gauge the potential engine response and intervention required for stable/optimal operation, the thermo-physical properties of the four syngas compositions and their constituent components are discussed in the current section. The thermo-physical properties are segregated into two groups, the first group addresses the basic properties arrived at based

Table 4 – Range and accuracy of the instruments used.

Instrument	Range	Accuracy
Fuel gas analyzer		
CO	0–100%	±0.05%
H_2	0–100%	±0.05%
CH_4	0–100%	±0.05%
CO_2	0–100%	±0.05%
O_2	0–025%	±0.005%
Cylinder pressure sensor	0–150 bar	±0.5 bar
Angle encoder		±0.25°
Venturi (C_d)		±1.0% (full scale)
Manometer		±1.00 mm
Optical speed sensor	0–20,000 rpm	±10 rpm
Thermocouple (K)	−200 to 1250 °C	>of 2.2 °C/0.75%
Watt-meter	0–100 kW	±1.0%

on gas composition and in-cylinder process conditions while the second group concentrates exclusively on the properties associated with the premixed mixture laminar flame.

Evaluation of calorific value, specific heat, thermal conductivity and diffusivity

The key thermo-physical properties of the four gas compositions and corresponding stoichiometric mixtures are evaluated and consolidated in Table 5. The properties like specific heat, thermal conductivity and viscosity are arrived at on mole fraction weighted average basis and curve fit coefficients based on molecular kinetic theory (for process conditions indicated in Table foot note). The specie thermal conductivity (k) and specie dynamic viscosity (μ) as a function of temperature (T) are estimated using the NASA curve fit expression and coefficients (A_k, B_k, C_k, D_k and A_μ, B_μ, C_μ, D_μ) as in equation (2).

$$\ln(k) = A_k \ln(T) + \frac{B_k}{T} + \frac{C_k}{T^2} + D_k \quad \ln(\mu) = A_\mu \ln(T) + \frac{B_\mu}{T} + \frac{C_\mu}{T^2} + D_\mu \tag{2}$$

The individual specie viscosity data is used in the formulation proposed by Wilke [44], as in equation (3), for estimating the mixture viscosity (μ_{mix}) while the mixture thermal conductivity (λ_{mix}) is estimated using a combination averaging formula proposed by Mathur et al. [45] as in equation (4).

$$\mu_{mix} = \sum_{i=1}^{i=n} \frac{\mu_i}{\frac{1}{x_i}\sum_{j=1}^{j=n} x_j \phi_{ij}} \quad \phi_{ij} = \frac{\left[1 + \left(\frac{\mu_i}{\mu_j}\right)^{1/2}\left(\frac{M_j}{M_i}\right)^{1/4}\right]^2}{\left(\frac{4}{\sqrt{2}}\right)\left[1 + \left(\frac{M_i}{M_j}\right)\right]^{1/2}} \tag{3}$$

$$\lambda_{mix} = \frac{1}{2}\left[\sum_{i=1}^{i=n} x_i \lambda_i + \frac{1}{\sum_{i=1}^{i=n} \frac{x_i}{\lambda_i}}\right] \tag{4}$$

Table 5 – Thermo-physical properties of syngas and stoichiometric mixtures.

Property	Units	C1	C2	C3	C4
Fuel properties					
Molecular weight	(kg/kMole)	26.12	24.98	23.96	21.85
Density (NTP[a])	(kg/m^3)	1.09	1.04	1.00	0.91
Calorific value	(MJ/kg)	3.14	4.17	5.28	7.55
	(MJ/m^3)	3.24	4.12	5.00	6.52
Specific heat	(kJ/kg^{-K})	1.15	1.20	1.28	1.43
Thermal conductivity	(mW/m^{-K})	35.9	40.2	46.7	56.3
Thermal diffusivity	(cm^2/s)	0.302	0.339	0.383	0.455
Stoichiometric air–fuel ratio	(kg/kg)	0.88	1.12	1.49	2.14
Fuel–air mixture properties corresponding to $\phi = 1.00$					
Molecular weight	(kg/kMole)	27.33	26.88	26.66	26.17
Density (NTP[a])	(kg/m^3)	1.08	1.06	1.05	1.03
Calorific value	(MJ/kg)	1.67	1.97	2.12	2.41
	(MJ/m^3)	1.80	2.09	2.24	2.49
Specific heat	(kJ/kg^{-K})	0.99	0.99	0.99	1.00
Thermal conductivity	(mW/m^{-K})	31.57	33.27	35.29	37.56
Thermal diffusivity	(cm^2/s)	0.296	0.317	0.337	0.363

[a] Temperature 298.15 K and Pressure 1.01325 bar.

The constant pressure specie specific heat ($\overline{C}_p$) and mixture specific heat ($\overline{C}_{p_{mix}}$) are evaluated from the expression as in equation (5).

$$\frac{\overline{C}_{p_i}}{R_u} = a_1 + a_2 T + a_3 T^2 + a_4 T^3 + a_5 T^4 \quad \overline{C}_{p_{mix}} = \sum_{i=1}^{i=n} x_i \overline{C}_{p_i} \tag{5}$$

Among the properties listed in Table 5, the mixture properties are of interest considering that the in-cylinder thermodynamic response depends on the fuel–air mixture rather than the fuel alone. The mixture calorific value, both on mass and volume basis, increases from C1 to C4. The highest calorific value at 2.41 MJ/kg is however lower than NG calorific value of 2.5 MJ/kg (conservative estimate based on 45 MJ/kg fuel calorific value and 17:1 air to fuel ratio). The reduced mixture energy density coupled with lower CR results in engine power de-rating [27,43]. Hydrogen with high thermal conductivity/diffusivity adds significantly to the mixture conductivity/diffusivity, potentially enhancing the convective heat losses from the engine. This aspect is dealt with in greater details in a subsequent section. The twin effects of de-rated engine operation (effectively part load operation for the available infrastructure) and higher convective heat losses are expected to adversely affect the engine performance in terms of its overall fuel conversion efficiency.

Laminar flame properties – temperature and structure

The fluid and thermodynamic conditions prevailing inside the engine cylinder are such that, the laminar flame thickness of the mixture is generally of the same order of magnitude or slightly higher than the prevalent Kolmogorov scale $\left(\frac{\delta_L}{l_k} \leq 1\right)$ [24]. As such, the structure of the turbulent flame in the cylinder is essentially one of highly wrinkled laminar flame (wrinkled laminar flame regime) [46]. Thus, analysis of laminar flame characteristics gives insight into the nature of combustion in the engine and allows assessing the influence on combustion phasing and hence on the ignition timing. Similarly, the adiabatic flame temperature permits establishing the upper limit of the thermodynamic efficiency.

In the current investigation, laminar flame characteristics for the four gas compositions are determined using the chemical kinetics package CHEMKIN [47] which simulates the detailed structure of a freely propagating one dimensional laminar flame in double infinity domain by solving for the relevant conservation equations. The GRI-Mech 3.0 reaction mechanism [48] involving 325 reactions (with 3 duplicates) and 53 species is used for the reaction kinetics. Different aspects related to the laminar flame characteristics are consolidated as below.

Adiabatic flame temperature

The variation of AFT with equivalence ratio at ambient (1 bar/300 K) and engine like (25 bar/700 K) conditions (typical motoring temperature and pressure for the considered engine configuration) are presented Fig. 2(a) and (b) respectively. The equivalence ratio at which the adiabatic flame temperature peaks and the corresponding temperature are explicitly indicated.

Some of the key findings from the AFT parametric analysis are presented below;

1. The AFT for the syngas compositions under consideration is lower than individual specie values. This is attributed to the presence of diluents CO_2 and N_2 in syngas, ranging from approximately 75% for C1 to about 40% for C4 (refer Table 2), influencing the gas calorific value (refer Table 5) and hence the AFT. Comparing the AFT among the syngas compositions, the dependence on calorific value is evident.
2. From ambient to engine like conditions (temperature and pressure increase of 400 K and 24 bar) the increase in the adiabatic flame temperature is in the range of 305 ± 10 K. A simple analysis for composition C4 indicates that at 1 bar pressure, an increase of unburned mixture temperature from 300 K to 700 K increases the adiabatic flame temperature by 218 K while at 300 K, increasing the unburned mixture pressure from 1 bar to 25 bar leads to a modest adiabatic flame temperature increase of only 32 K. Thus, the increase in adiabatic flame temperature from ambient to engine like conditions is primarily attributed to the increase in unburned gas temperature with pressure having very nominal effect, restricted only to suppression of dissociation of the gaseous species.
3. In the operating equivalence ratio regime of interest i.e., 1.0 ± 0.2, it can be observed that for both ambient and engine like operating conditions, the difference in adiabatic flame temperature between the considered compositions broadly remains constant. No particular fuel specific sensitivity to equivalence ratio is observed.

Summarizing the above results, it is evident that the adiabatic flame temperature(s) being lower than the constituent component temperature(s) over a range of thermodynamic conditions and equivalence ratio, any (potential) higher cooling load observed during experimental investigations, cannot be attributed to the peak cylinder temperature for the range of compositions considered in this study.

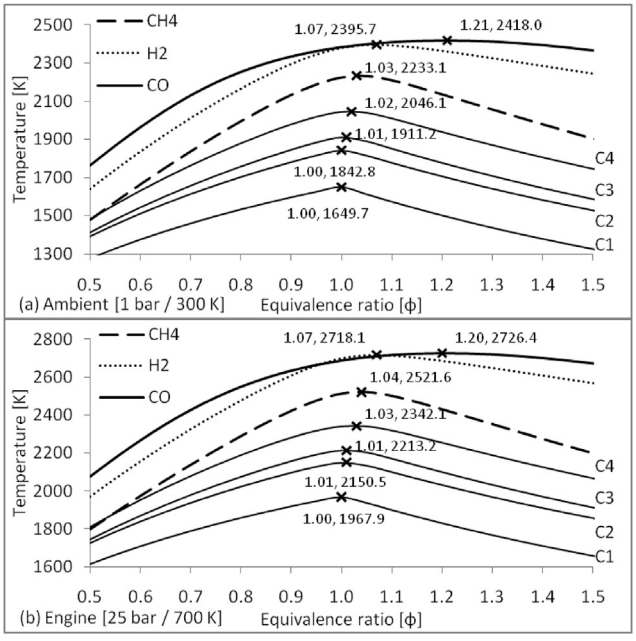

Fig. 2 – Variation of adiabatic flame temperature with equivalence ratio for syngas and constituent species.

Flame structure

The detailed laminar flame structure for stoichiometric mixture under 1 bar pressure and 300 K temperature (ambient condition) is consolidated in Fig. 3(a)–(d) for the four syngas compositions used in the current investigation. The flame structure is described based on the variation of temperature, net heat release from the gas phase reactions and heat release from the four highest heat release contributing reactions against the reference linear coordinate. The flame structure under engine like conditions (representative conditions; 25 bar pressure and 700 K temperature) has also been considered for analysis as in Fig. 4.

The key feature explicitly evident from Figs. 3 and 4 is the increase in flame temperature for gas compositions C1 to C4 and higher temperatures under engine like conditions. From the heat generation rate profiles, the influence of fuel composition (especially H_2) on the reaction kinetics is clearly evident. From Figs. 3 and 4 it can be observed that the net heat generation rate from the gas phase reactions increases by an order of magnitude from C1 to C4 resulting in AFT increase by about 400 K for both ambient and engine like conditions. Between engine and ambient conditions, AFT temperature difference of about 250 K is observed. The increase in net heat generation rate with increasing H_2 fraction is attributed to the significant increase in the overall reactivity. This is evident from the comparison of forward rate of $OH + H_2 \leftrightarrow H + H_2O$ reaction for stoichiometric mixture of the four syngas compositions under ambient and engine like conditions as consolidated in Table 6.

Increase in mixture H_2 fraction, apart from enhancing the heat generation rate, also reduces the thickness over which the heat release take place, suggesting flame thickness reduction. Evaluating the total flame thickness as the ratio of temperature rise in the flame to the peak temperature gradient [49,50]; about 50% reduction in the overall flame thickness is observed from C1 to C4. Similarly, comparing the flame thickness for ambient and engine like conditions, an order of magnitude reduction is evident (flame thickness magnitudes indicated as inset data of Figs. 3 and 4). The observed behavior is explained from the flame thickness hypothesis proposed by Glassman [51] as in equation (6). It is observed that, with an increase in H_2 or change in the conditions from ambient to engine like conditions, the increase in the product of density and thermal diffusivity ($\rho\alpha$) is nominal (refer Table 5) as compared to the increase in overall rate of reaction, hence the reduction in flame thickness.

$$\delta_{flame} = \sqrt{\frac{\rho\alpha}{RoR}} \tag{6}$$

While the reduction in the overall flame thickness is explicitly evident, a simple analysis of the temperature and net heat release profile suggests significant influence of H_2 on the laminar flame pre-heat zone. Comparing the heat release and temperature profiles, it is evident that, with

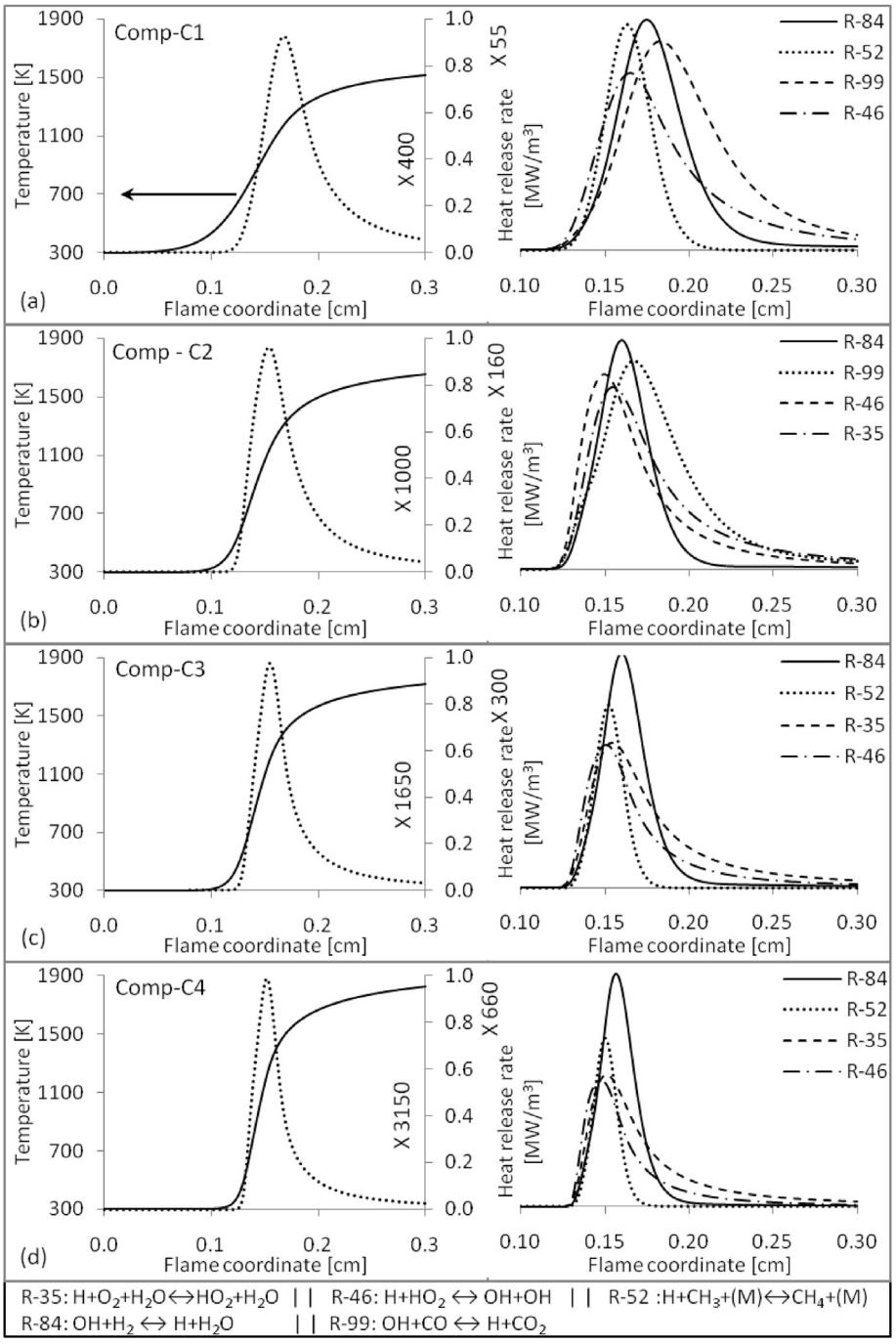

Fig. 3 – Laminar flame structure under ambient conditions for stoichiometric mixtures.

increasing H_2 fraction, the heat release starts at temperatures much closer to un-burned gas temperature, suggesting a reduction in the preheat zone thickness. Comparison of the flame temperature at net heat release rate of 0.1 MW/m^3 for the four compositions indicates the temperature to be 449 K for C1 reducing to 322 K for C4, confirming the reduction of preheat zone thickness. This reduction is directly attributed to the lower than unity Lewis number for H_2 and some of the key radicals associated with H_2 combustion (refer Table 7). Lower than unity Lewis number results in preferential specie/radicals diffusion into the unburned mixture [52,53] and with some of the species having very high reactivity, reaction of the mixture is initiated at much lower temperatures very early into thermal heating. With increasing mixture H_2 fraction, rapid buildup of reactive species ahead of the flame ensures initiation of heat release at lower temperatures.

Analyzing the key participating reactions, it is observed that reaction 84 ($OH + H_2 = H + H_2O$), basically a chain reaction and the primary source of H radical generation, is the key

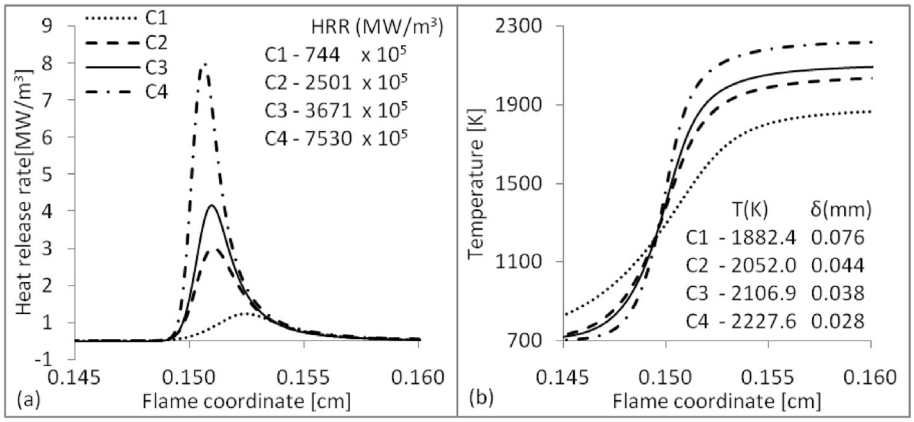

Fig. 4 – Laminar flame structure under engine like conditions for $\phi = 0.85$.

reaction for all the four compositions with maximum at about 10 microns beyond the peak net heat release position. A portion of generated H radicals diffuses rapidly into the incoming unburned mixture and initiates the key leading edge reaction with HO2 (R-46) producing two OH radicals for each H consumed. With increasing H_2 fraction in the fuel, the rate of reaction 84 increases, increasing the concentration of *H* radicals and their subsequent diffusion into the preheat zone. The *H* are rapidly consumed in one of the many reactions [55] resulting in the reduction of preheat zone thickness.

It is evident from the foregone discussions that with increasing mixture H_2 fraction, H based radicals being to dominate resulting in a lower than unity Lewis number (refer Table 7) and reduced laminar flame thickness. The direct consequence of the above two factors is the appearance and subsequent increase of flame surface instabilities culminating in flame cellularity [56–58]. The weaker influence of curvature and increased intensity of baroclinic torque (due to reduced flame thickness) and competing effects of thermal and mass diffusion ($Le < 1$) [56] induce instability and cellularity in the flame structure. The transition from smooth to cellular structure is important considering that extended wrinkling of the flame due to cellularity accelerates the flame significantly [59] having a turbulence like influence in enhancing the flame speed. This has been brought out explicitly in a work by Toshiaki et al. [60] who have proposed a correlation for turbulent burning velocity in terms of Reynolds and Lewis number. The most significant influence of such flame cellularity and corresponding flame acceleration is expected to be on the engine thermo-kinematic response considering that the onset of flame instability and cellularity is a complex function of mixture H_2 fraction and prevailing thermodynamic conditions [61].

Table 6 – Forward rate of $OH + H_2 \leftrightarrow H + H_2O$ reaction under ambient and engine like conditions.

	C1	C2	C3	C4
	mole/cm^{3-s}			
01 bar–300 K	4.40×10^{-5}	2.03×10^{-4}	3.89×10^{-4}	1.11×10^{-3}
01 bar–700 K	6.46×10^{-4}	7.88×10^{-4}	1.37×10^{-3}	4.13×10^{-3}
25 bar–300 K	3.68×10^{-5}	1.15×10^{-3}	4.84×10^{-3}	3.98×10^{-2}
25 bar–700 K	4.60×10^{-3}	4.21×10^{-2}	1.22×10^{-1}	5.03×10^{-1}

Table 7 – Lewis number for typical hydrogen and key hydrogen combustion radicals [54].

Φ	H_2	*O*	*H*	*OH*
0.7	0.31	0.72	0.18	0.74
1.0	0.33	0.78	0.20	0.79
1.4	0.37	0.89	0.23	0.91

Flame propagation

The variation of laminar flame speed with mixture quality for the four syngas compositions and CH_4 under ambient and engine like conditions is consolidated in Fig. 5(a) and (b) respectively. In Fig. 5, the peak flame speed and corresponding equivalence ratio are explicitly identified and the laminar flame speed corresponding to equivalence ratio of 0.85 (the considered operating condition) is included as inset data.

An increase in laminar flame speed with increasing H_2 fraction is explicitly evident from Fig. 5 and is primarily attributed to the increase in the overall reactivity. Based on the assessment of the total heat release rate for the four gas compositions (as indicated in Figs. 3 and 4) it is evident that an increase in H_2 fraction in the mixture leads to a significant increase in the peak heat release rate and a shift in the peak heat release position closer to the fresh incoming mixture. Between C1 and C4 while the mixture H_2 fraction doubles, the peak heat release rate experiences a near 10 fold increase. The steep temperature gradient due to higher heat release rates and higher diffusivity of key free radicals leads to an increase in laminar flame speeds with increasing mixture H_2 fraction [62–64]. While the laminar flame speed increases with mixture H_2 fraction, it is interesting to note that the increase is significant for low mixture H_2 fractions as compared to high mixture H_2 fractions, especially in the vicinity of stoichiometry. Considering the particular case of laminar flame speed at $\phi = 0.85$, it can be observed that, between C1 and C2, for mixture H_2 fraction increase from 7.1% to 9.1% (an increase of 2% absolute) while the laminar flame speed increases by 100%,

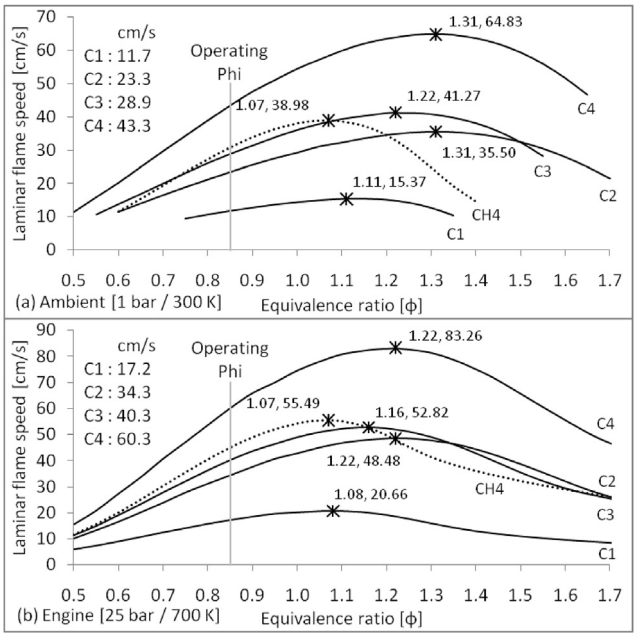

Fig. 5 – Variation of laminar flame speed with equivalence ratio under ambient and engine like conditions.

between C3 and C4, for mixture H_2 fraction increase from 11.6% to 14.2% (an increase of 2.6% absolute) the laminar flame speed increases by only 50%. The rather sharp increase in laminar flame speed with H_2 fraction in the low H_2 concentration regime is primarily attributed to the change in *CO* reaction kinetics. In the low H_2 concentration regime, increase in H_2 fraction leads to the slow third body *CO* oxidation reaction ($O + CO + (M) \leftrightarrow CO_2 + (M)$) giving way to the fast *CO* oxidation by *OH* ($OH + CO \leftrightarrow CO_2 + H$) [50]. However, at higher concentration levels, no such rate boost is provided since the key reactions are all controlled by radicals containing *H* atoms. Thus, flame speed increase in the high H_2 concentration regime is predominantly due to enhanced diffusivity. This response is evident in the laminar flame structure description for the four compositions (refer Fig. 3). It can be observed that for compositions C1 and C2, while *CO* oxidation (through OH, R-99) is a key reaction the same does not figure in C3 and C4 structure, indicating the reduced significance. The key reactions are driven by radicals containing *H* atoms.

The practical consequence of laminar flame speed variation at the operating equivalence ratio is on the ignition timing. Under the assumed condition of similar turbulent intensity in the engine for all the four compositions, compositions C1 and C2 require ignition advance while compositions C3 and C4 would require ignition retard with respect to typical NG operation to position the engine to deliver maximum brake power.

Results and discussions

The results of the current investigation involving syngas fueled engine operation are consolidated and discussed in two broad segments;

a. Maximum brake torque ignition timing and engine performance analysis dealing primarily with energy balance and
b. in-cylinder response addressing the pressure rise and heat release characteristics.

The results of engine performance analysis and energy balance form the basis for addressing the consolidated influence of mixture H_2 fraction on the engine performance while the results of in-cylinder investigation address the influence of H_2 on the thermo-kinematic response, quantified in terms of the apparent heat release profile.

Engine performance

Maximum brake torque ignition timing and peak load

The strong dependence of engine thermo-kinematic response on the fuel thermo-physical properties dictates the need for establishing the MBT ignition timing whenever the gas composition changes. The conventional methodology of establishing MBT ignition timing involves taking the engine through a spark sweep i.e., operating the engine at different ignition timings in a pre-determined range. The ignition angle which delivers knock free peak load is designated as the MBT ignition timing. Real time acquisition and processing of in-cylinder pressure traces permit adopting a more refined approach towards establishing the MBT timing as described below.

The energy conversion process in an engine through finite heat release dictates the in-cylinder pressure to peak beyond the TDC. Literature reports the position of peak pressure for conventional fuels to be in the vicinity of 15° after TDC [21,65]. In working with *PG*, the authors have observed the MBT ignition timing around 13° after TDC [26,28]. In the current investigation, starting with composition C1 and following on the previous experience, the ignition timing was first adjusted to have the position of peak pressure based on the 50 cycle ensemble average pressure profile between 12 and 15° after the TDC. The choice of ensemble averaging and use of 50 cycles has been discussed elsewhere [28]. Subsequently, fine adjustment of ignition angle to derive normal operation (through crank angle processing) maximum power permitted fixing the MBT timing and the corresponding peak load. Having established the MBT ignition timing for composition C1, subsequent ignition timing tuning for other compositions were directed towards retarded ignition settings considering the higher laminar flame speeds (refer Fig. 5).

The expected and achieved peak load and MBT ignition timing for the four compositions are listed in Table 8. The estimated peak load is based on the power per unit swept volume analysis considering 4.65 kWe/l of swept volume for standard stoichiometric *PG*–air mixture (LCV-Mixture: 2.17 MJ/kg). Sample calculation for composition C1 is presented below. The value 4.65 kWe/l is based on previous operational experience on naturally aspirated engines [26,30,66] fueled with *PG*.

$$\text{Load per unit swept volume(C1)} = \frac{\text{Actual mixture A/F(1.54)}}{\text{PG stoichiometric A/F(2.17)}} * 4.65 = 3.3\ \text{kWe/l}$$

Table 8 – Peak load achieved and maximum brake torque ignition timing.

		C1	C2	C3	C4
Peak load achieved	kWe	5.4	6.0	6.4	7.1
Peak load estimated	kWe	5.5	6.4	6.9	7.7
MBT Ignition timing	deg bTDC	25	23	20	18
Position of peak pressure	deg aTDC	13	13	10	09

Addressing the MBT ignition timing, mixture H_2 fraction increase demands retarding the ignition setting, attributed to the increase in the laminar flame speed (refer Fig. 5) and dictated by the need for positioning the combustion phasing to maximize thermal to mechanical energy conversion. The peak supported load, along expected lines, follows the trend of lower calorific value. Of particular interest is the maximum difference between the estimated and achieved load being around 7.0% (for composition C3), highlighting the superior nature of the load estimation methodology arriving from simple analysis. Another feature of interest is the fact that, with increasing H_2 fraction, while MBT operation requires ignition retard, increasingly closer positioning of the peak pressure to the TDC is also observed. While engine combustion literature suggests retarded ignition setting with higher laminar flame speeds to ensure nearly invariant post TDC combustion phasing [65], the presence of H_2 in the mixture, as evident from the current investigation, influences the position of the peak pressure. This has a particularly significant influence on the engine diagnostics and control [28]. The variation in combustion phasing brought about by the presence of H_2 is discussed in details in a subsequent section dealing with in-cylinder pressure traces.

The respective MBT ignition timing established for peak load operation is retained for part load operation.

Brake specific energy consumption and thermal efficiency

The brake specific fuel and energy consumption and brake thermal efficiency data for peak and part load operation are consolidated in Table 9. For peak load operation, with an increase in the mixture calorific value, the brake specific fuel and energy consumption decrease while the brake thermal efficiency increases upto composition C3 and subsequently a small drop of 0.3% (absolute) is observed for composition C4. The trend is along expected lines considering the support from governing thermodynamic parameters like adiabatic flame temperature and shorter combustion duration due to higher laminar flame speeds. The slight reduction in efficiency from C3 to C4 overcoming factors favoring an increase is unexpected and is addressed subsequently by drawing up the energy balance.

To assess the relative performance of the engine with the four compositions, performance of sub 10 kWe generator sets fueled with NG (KOHLER, GE and BRIGGS and STRATTON engines were considered) were analyzed. The typical brake specific energy consumption for such engines is around 19 ± 1 MJ/kWh with corresponding efficiency of around 19.0 ± 0.5%, comparable to engine performance with C1 and C2. It is important to note that while the laminar flame speed and adiabatic flame temperature for compositions C1 and C2

Table 9 – Engine performance at full and part load operation.

		C1	C2	C3	C4
Peak load operation					
Load	kWe	5.4	6.0	6.4	7.1
BSFC	g/kWh	6235	4285	2887	2050
BSEC	MJ/kWh	19.58	17.87	15.24	15.48
η_{bth}	%	18.4	20.1	23.6	23.3
Part load operation – 5.4 kWe					
De-rating from peak load	kWe (%)	0.0 (0.0)	0.6 (11.1)	1.0 (18.5)	1.7 (31.5)
BSFC	g/kWh	6235.0	4496.3	3224.0	2253.7
BSEC	MJ/kWh	19.58	18.75	17.02	17.01
η_{bth}	%	18.4	19.3	20.8	19.7
Average suction pressure	bar	0.678	0.669	0.612	0.603

are lower than that of NG (refer Figs. 2 and 5) the specific fuel consumption and efficiency are comparable. This is attributed to the lower CR of 8.5 (a reduction of 2.5 units compared to the current test engine on PG) on the considered NG engines leading to some loss in performance.

On part load performance, the reduction in brake thermal efficiency from C1 to C4 is attributed to increased pumping losses at part load operation leading to a reduction in the net indicated work per cycle [21,67]. Further, lower intake pressures also lead to a reduction in the effective CR [68] enhancing the loss of efficiency. The qualitative statement of increasing pumping load is analyzed in a subsequent section.

Energy flow analysis and addressing the cooling load

The energy balance, involving quantifying the various streams into which the input energy gets distributed, is consolidated in Table 10 for the peak and part load operation.

Analyzing the peak load energy balance data for the four compositions indicates an interesting trend. The overall cooling load for the four gas compositions is between 7 and 12% higher than the corresponding values for gasoline operation (17–26%; refer [21,69]) and approaches/surpass the general upper limit for typical diesel operation (16–35%; refer [21,70]). Further, while the overall cooling loads are higher for syngas fueled operation, an increase in the cooling load with mixture H_2 fraction is also observed. Addressing the higher cooling load for syngas fueled operation, in the analysis of syngas basic properties (refer Evaluation of calorific value, specific heat, thermal conductivity and diffusivity section), it was observed that the mixture thermal conductivity/diffusivity increases with H_2 fraction and is expected to proportionately increase the convective heat loss from the engine. This argument of H_2 enhancing the convective cooling load can be strengthened by quantifying the variation of gas side convective heat transfer coefficient and heat flux with mixture H_2 fraction. Towards the same, the gas side convective heat flux ($\dot{Q}''''_{wht}$) between the working fluid and the constraining walls is estimated using the Newton's cooling law as in equation (7) where, $h_{c,g}$ is the gas side convective heat transfer coefficient [71,72] while $\overline{T}_g$ and $\overline{T}_w$ represent the cylinder average gas temperature and cycle average wall temperature respectively. The convective heat transfer coefficient

Table 10 – Engine energy balance and supporting information.

		C1	C2	C3	C4
Peak load energy balance					
Input energy	kW (%)	29.37 (100)	29.78 (100)	27.09 (100)	30.53 (100)
Electrical output	kW (%)	5.40 (18.4)	6.00 (20.1)	6.40 (23.6)	7.10 (23.3)
Cooling load	kW (%)	9.85 (33.5)	10.35 (34.8)	9.95 (36.7)	11.50 (37.7)
Exhaust thermal enthalpy	kW (%)	9.51 (32.4)	8.73 (29.3)	7.30 (27.0)	7.75 (25.4)
Supplementary energy balance data					
Exhaust gas temperature	°C	441	455	457	485
Exhaust flow rate	kg/h	68.55	60.28	51.22	50.86
Part load energy balance					
Input energy	kW (%)	29.37 (100)	28.0 (100)	25.9 (100)	27.35 (100)
Electrical output	kW (%)	5.40 (18.4)	5.40 (19.3)	5.40 (20.8)	5.40 (19.7)
Cooling load	kW (%)	9.85 (33.5)	9.62 (34.4)	8.90 (34.3)	10.0 (36.6)
Exhaust thermal enthalpy	kW (%)	9.46 (32.2)	7.98 (27.2)	6.56 (22.3)	5.90 (20.1)
Supplementary energy balance data					
Exhaust gas temperature	°C	441	450	438	440
Exhaust flow rate	kg/h	68.55	56.31	47.88	42.77

is estimated based on the empirical correlation relating the Nusselt (*Nu*) number to the Reynolds (*Re*) and Prandtl number (*Pr*) as in equation (8) [73] (relevant parameters described in Table 11).

$$\dot{Q}''_{wht} = h_{c,g}\left[\overline{T}_g - \overline{T}_w\right] \tag{7}$$

$$Nu = a\mathrm{Re}^{\alpha}\mathrm{Pr}^{\beta} = \xi\mathrm{Re}^{\alpha} \;\; ; \quad h_{c,g} = \xi\frac{k}{B}\mathrm{Re}^{\alpha} = \xi\frac{k}{B}\left[\frac{\rho VB}{\mu}\right]^{\alpha} \tag{8}$$

The compression process heat flux as a function of crank angle for stoichiometric mixtures of the four gas compositions is consolidated in Fig. 6(a) while the same for three stoichiometric CH_4–H_2 mixtures is consolidated in Fig. 6(b). The percentage contribution of H_2 to the mixture in mass, volume and energy fraction is included as inset data.

An increase in H_2 fraction from 25% to 75% in the CH_4–H_2 mixture leads to about 20% increase in the peak convective heat flux (from 0.437 MW/m^2 to 0.521 MW/m^2) as indicated in Fig. 6(a). Extending the analysis to the four syngas compositions used in the present study (refer Fig. 6(b)), an increase in the convective heat flux with H_2 fraction is observed. The heat flux at 0.420 MW/m^2 for syngas composition C1 increases to 0.478 MW/m^2 for composition C4, an increase of about 15%. This manifests as an increase in the cooling load from composition C1 to C4, attributed to the increase in mixture H_2 fraction. This aspect has also been addressed by Saleel et al. [74] based on the second low analysis of an H_2 fueled engine.

It may also be noted that from C1 to C4, while the peak supported load and exhaust gas temperature increase (refer Table 10), the fraction of energy discharged as exhaust enthalpy decreases. This response can be addressed based on the analysis of the governing mathematical expression (equation (9)) used for estimating the exhaust enthalpy.

$$\dot{Q}_{exh} = \dot{m}_{exh}C_{p-exh}(T_{exh} - T_{amb}) \tag{9}$$

Using the data from Table 10 it can be observed that the exhaust gas flow rate and temperature have opposite trends from composition C1 to C4 and the reduction in exhaust flow rate is significantly higher (26%) as compared to the increase in the temperature (16%). This leads to a reduction in the exhaust enthalpy from composition C1 to C4 (refer equation (9)).

Engine cooling load – a side note

While the foregone discussion on energy balance explicitly establishes the influence of H_2 in enhancing the cooling load which is also supported by the analysis of syngas thermo-physical properties (refer Syngas thermo-physical properties section), two pertinent features, as identified below require particular attention.

1. The calculated convective heat transfer coefficient and peak heat flux (at TDC) for pure CH_4 and syngas C1 are very similar (C1 heat flux is higher only by 0.005 MW/m^2 as compared to CH_4). This suggests that for similar in-cylinder conditions, the convective heat losses for C1 fueled operation would be only slightly higher than that due to CH_4 fueled operation.
2. Considering the actual engine operation, with the adiabatic flame temperature and energy density for C1 being

Table 11 – Heat transfer coefficient estimation – parameter description and magnitudes.

Parameter	Remarks
Thermal conductivity, k	$f(T)$; Estimated from kinetic theory curve-fit coefficients
Dynamic viscosity, μ	$f(T)$; Estimated from kinetic theory curve-fit coefficients
Characteristic length, B	Engine bore diameter (0.102 m)
Characteristic speed, V	Mean piston speed (6 m/s)
Working fluid density, ρ	$f(\theta)$; Ratio of mass to volume
Coefficients α and ξ	0.7 and 0.5 respectively; $0.35 \leq \xi \leq 0.80$; refer [21]

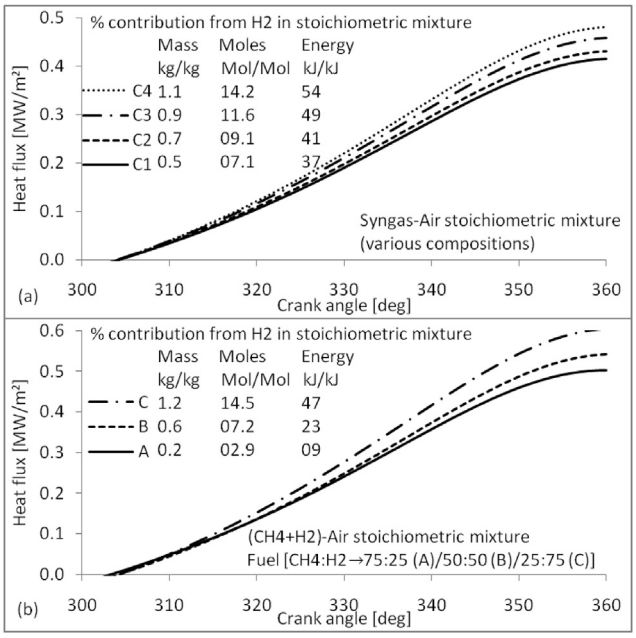

Fig. 6 – Influence of gas composition on the engine convective heat flux.

significantly lower than CH_4 (refer Table 2) and the engine operating lean, the in-cylinder thermal conditions for C1 operation are expected to be significantly dilute as compared to CH_4 fueled operating.

Considering the divergent conditions prevailing in the engine pertaining to convective heat transfer as brought out by the listed points, theoretically, the heat losses for typical CH_4 operation and Syngas C1 should be very similar, to say the least. Measurements however reveal significantly higher cooling loads for syngas fueled operation (refer Table 10). It is apparent from the above analysis that the convective heat flux and hence the engine cooling load are influenced by more than one parameters. While the current work addresses the influence of thermo-physical properties on the heat flux, both qualitatively and quantitatively, preliminary analysis based on equation (8) (necessitated by the above observation) indicates to the potential influence of turbulence. Considering that syngas fueled experience has always been with diesel adopted engines, as also in the current case, the potential role of adopted in-cylinder geometry in enhancing the heat flux, through higher in-cylinder turbulence, requires a detailed analysis, not in the scope of the current work.

In-cylinder investigations

Acquisition of in-cylinder pressure data permits (a) extending the generic performance analysis to include the indicated/pumping response and (b) the analysis of engine thermo-kinematic response, one of the key mandates of the current investigation. These two aspects are discussed in the following sections.

Indicated and pumping load analysis

In the analysis of brake thermal performance of the engine for the four compositions (refer Brake specific energy consumption and thermal efficiency section) it was observed that, with increasing H_2 fraction (moving from C1 to C4), while the brake thermal efficiency increased for full load operation, it decreased for part load operation. The part load behavior is sought to be analyzed through the indicated parameters derived from in-cylinder pressure traces as quantified in Table 12. One of the key features of the indicated data is the significant reduction in mechanical efficiency on moving from C1 to C4, the maximum being 66.35% against typical values of around 90%. The under 70% efficiency is typical of engine operation in the sub 30% operational load regime [21]. The reduction in mechanical efficiency causes a commensurate reduction in the brake thermal efficiency.

The reduction in mechanical efficiency (from C1 to C4) for the fixed load of 5.4 kWe is primarily attributed to the increase in pumping losses caused by higher throttle work ($[P_e - P_i]V_d$, restriction experienced external to the cylinder), due to reduced throttle opening as evident from Fig. 7(a). The increase in throttle work is significant to overcome the reduction in valve flow work (restriction attributed to the flow through the valves) at part load, with the net effect being an increase in the pumping losses. The other key factor contributing to in-cylinder losses is the higher in-cylinder pressure for compositions with higher H_2 fraction (at the same load of 5.4 kWe) as evident from Fig. 7(b) and quantified in Table 12. Higher in-cylinder pressures lead to enhancement in the rubbing friction [75,76] leading to enhanced losses. With respect to the rubbing friction, it is important to note that the baseline diesel piston having three piston rings is adapted for gasoline operation as against two piston rings typical for SI operation (refer Fig. 8). The increasing in-cylinder pressures coupled with more number of piston rings effectively amplifies the frictional losses. Thus, the increase in throttle work and rubbing friction leads to a reduction in the mechanical and hence brake thermal efficiency from composition C1 to C4 under part load conditions.

Thermo-kinematic response

Maximum brake torque combustion phasing. A review of literature pertaining to MBT combustion phasing for engine operation with conventional fuels indicates invariance of certain geometric inflection characteristics (known as combustion descriptors) corresponding to pressure-crank angle and heat release-crank angle traces [21]. The (ensemble average) position of peak pressure and maximum heat release

Table 12 – Part load pressure trace derived mean effective pressure parameters.

		C1	C2	C3	C4
IMEP-Gross	bar	4.177	4.235	4.457	4.500
IMEP-Pumping	bar	0.284	0.278	0.302	0.319
IMEP-Nett	bar	3.893	3.957	4.155	4.181
Mechanical efficiency	%	66.35	65.45	62.33	61.94
Throttle work	J/cycle	24.27	25.52	27.69	29.94
Peak cylinder pressure	Bar	24.27	25.25	27.16	30.35

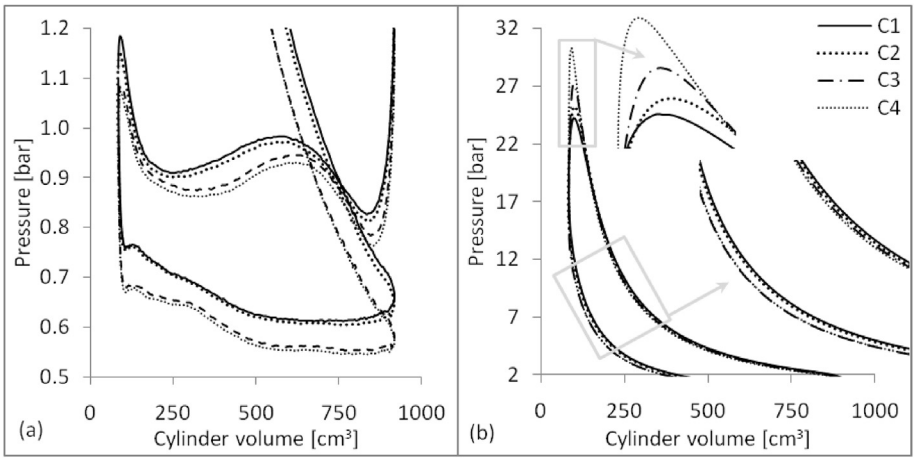

Fig. 7 – Part load PV diagram (a) gas exchange and (b) compression–expansion process (magnified view not correspond to the coordinate scale).

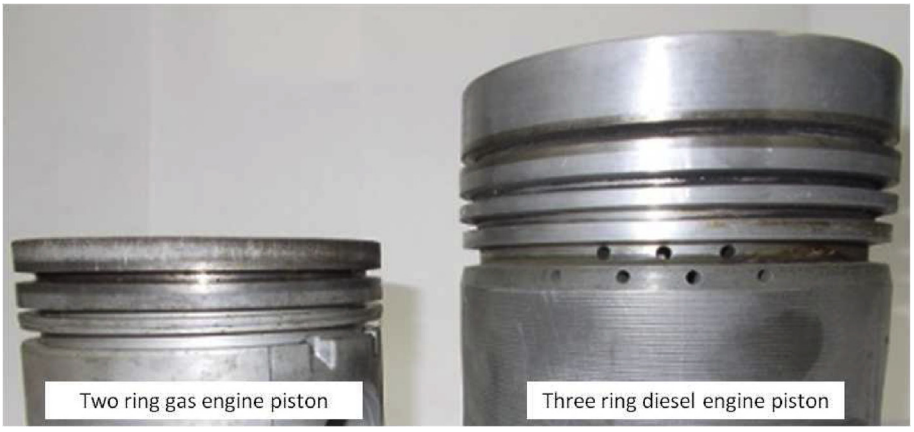

Fig. 8 – Number of rings on typical gasoline and diesel engine pistons.

rate are two key combustion descriptors that qualify the combustion phasing for MBT operation [65]. Hubbard et al. [77], and Heywood [21] have reported the position of peak pressure to be around 15 and 16° after TDC respectively for MBT operation with conventional fuels. The corresponding position of maximum heat release is reported to be around 9° after TDC [65,78]. The mentioned descriptors are so well established in terms of invariance and repeatability at MBT operation that they are used as diagnostic parameters to assess ignition timing offset (if any) from optimal conditions and to restore the engine for MBT operation through a feedback control logic [65]. While the identified values hold good for conventional fuels, in a work involving PG fueled engine operation, the authors observed a shift in the combustion phasing towards TDC for MBT operation, as compared to typical gasoline operation [28]. A detailed analysis attributed the advance in combustion phasing to fuel H_2 fraction [28]. As a consequence of the phase shift, an advancement of the position of peak pressure and maximum heat release by about 2° crank angle was observed. Following up on the observed results with PG, the current section addresses the influence of syngas H_2 fraction on the combustion descriptors at MBT. The influence of syngas H_2 fraction on the position of peak pressure and maximum heat release rate are consolidated in Fig. 9 for both peak and part load operation. The respective descriptor values for the four compositions are included as inset data along with the literature reported value for conventional higher hydrocarbon fuel (in bordered boxes).

A general shift in the combustion phasing towards TDC with increasing H_2 fraction is evident with both, the position of peak pressure and maximum heat release rate being placed closer to the TDC. The advanced phasing is interesting considering that ignition timing has been retarded to account for the higher laminar flame speeds and points to a significant increase in heat release rate in the engine. This is evident from Fig. 9(b) and (d) where the differential heat release rate for the four compositions are presented. It is evident from the above analysis that the magnitude of combustion descriptors for

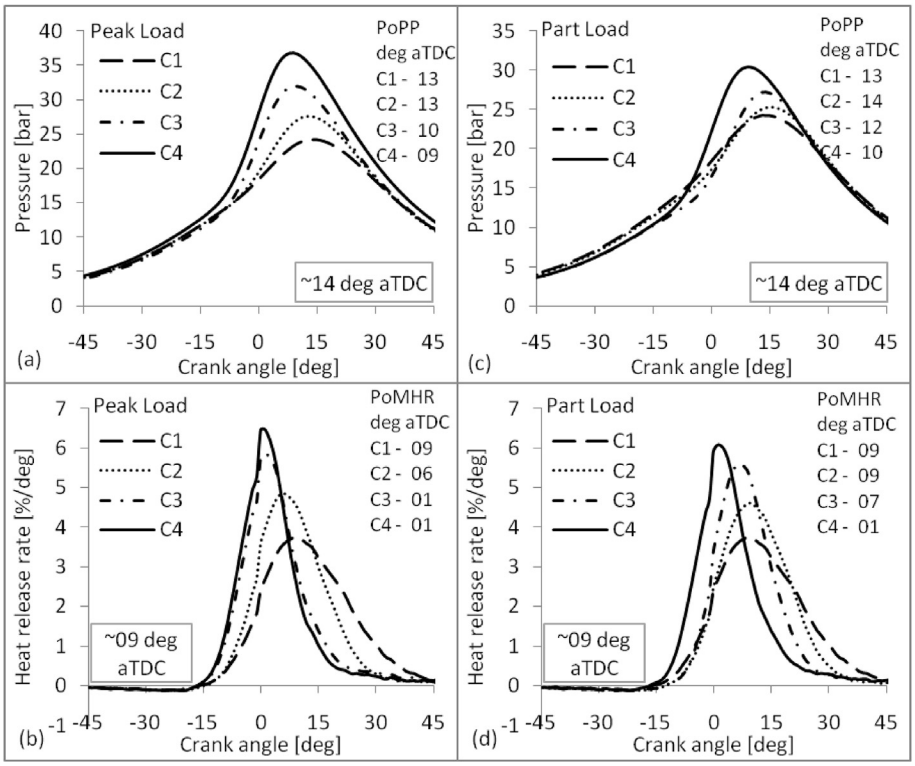

Fig. 9 – Influence of syngas H_2 fraction on the position of peak pressure and maximum heat release rate at part and full load operation.

conventional high calorific value fuels (being used as control signal for tuning the ignition timing for MBT operation) cannot be treated as sacrosanct numbers applicable throughout the complete spectrum of fuels. This is especially true if the general thermo-physical properties of the fuel are significantly different from those of conventional fuels.

While the influence of syngas H_2 fraction on the combustion phasing is explicitly evident from the foregone discussion, the response itself can be better appreciated by analyzing the heat release pattern considering that the in-cylinder pressure is a manifestation of in-cylinder heat release. The MBT heat release pattern for the four compositions is consolidated in the following discussion.

Heat release pattern. The cumulative heat release pattern for the four gas compositions is consolidated in Fig. 10 wherein the advanced phasing of combustion with increasing H_2 fraction is clearly observed for both part and full load operation. The general shift in the combustion phasing is again attributed to the enhanced mixture reactivity and heat release rate as discussed in Syngas thermo-physical properties section.

While the advanced phasing addresses the shift in combustion descriptors, the heat release profiles indicate an interesting trend, especially near the terminal phase. With increasing syngas H_2 fraction, while the first half heat release rate is significantly higher (consistent with the mixture reactivity), the second half, especially the post 80% regime tends to become sluggish. This is consistent with the observation on *PG* fueled operation (refer Fig. 1) [28]. Towards analyzing this response, the heat release regime is segregated into the initial flame development phase (10% of heat release), the rapid burn phase (10%–90% of heat release) and the terminal phase (from 90% to 98%). The terminal phase culmination is set at 98% considering the uncertainty involved in exact determination of completion of combustion angle [79–82]. The duration of the three stages of combustion in absolute degrees and fraction of full cycle (%) for the four compositions are consolidated in Fig. 11 and the responses analyzed.

With increasing H_2 fraction, while the minimum ignition energy required reduces, the spark energy remains constant for all the four compositions (except for the change accompanying charge capacitance variation) and the fraction of energy in excess of the minimum required increases. The increase in the electrical energy leads to the establishment of a larger flame kernel with higher mean temperature that transits faster into a turbulent chemical flame [85,87] leading to a reduction in the initial flame development period. The near invariant initial burn time for engine operation at 5.4 kWe is attributed to the increased dilution of the mixture with residual gas fractions [88,89] (due to increasing part load operation with increase in mixture H_2 fraction; refer Table 9).

2. **Fast burn phase:** Response of the fast burn phase of combustion is along expected lines with the combustion duration decreasing with an increasing in mixture H_2

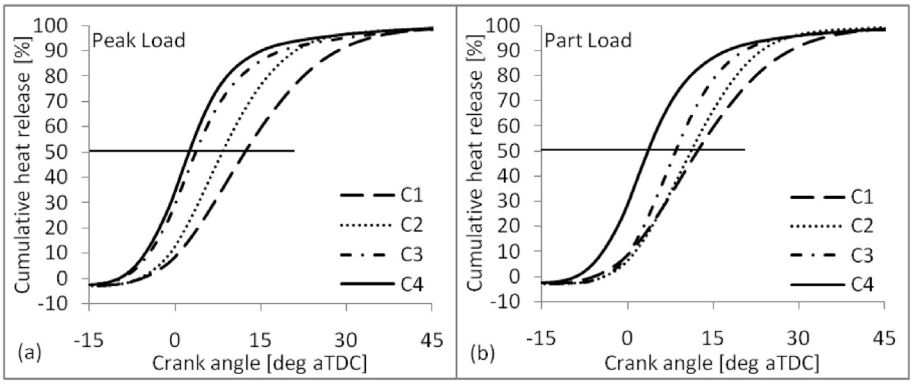

Fig. 10 – MBT cumulative heat release for the four syngas compositions at peak and part load operation.

fraction. The reduction is significant (~17%) for full load operation as compared to part load operation (~7%). Analysis of the nature of premixed turbulent combustion prevalent in typical engine like environments is useful to describe the observed trend. Photographic evidence based on schlieren/shadowgraphy techniques [90], laser scattering techniques [91,92] and comparison of laminar flame thickness – Kolmogorov scale as in Borghi–Peters diagrams [93,94] indicates the combustion in SI IC engines to be mostly being in the flamelet (wrinkled laminar flame) regime and some times extending to flamelet in eddies regime [24,46] depending on the operating condition. In the flamelet regime, while the eddies wrinkle the thin flame front, the combustion itself is at the characteristic laminar flame speed. Wrinkling of the flame front leads to the formation of islands or peninsular regions of unburned mixture [21,23,91,95,96] increasing the flame area and the unburned mixture consumption rate. As such the the influence of turbulence is reduced to wrinkling the flame front with the actual burning still governed by the mixture thermo-physical properties. The essence of the flamelet regime has been captured by various researchers as below (Damkohler model [24]), (Clavin and Williams model [24]), (Klimov model [24]).

$$S_t = S_L + V_{rms} \tag{11}$$

$$S_t = S_L + S_L V_{rms}^2 \tag{12}$$

$$S_t = 3.5 S_L^{0.3} V_{rms}^{0.7} \tag{13}$$

As evident from the above argument, for similar turbulence conditions in the engine cylinder, the burning rate directly depends on the laminar flame speed. Thus, the reduction in fast burning duration from C1 to C4 can be attributed to the increasing H_2 fraction and higher peak in-cylinder temperature (due to increasing peak supported loads) both of which increase the laminar flame speed. As for the part load operation, due to increasing levels of mixture dilution with residual gases, the influence of H_2 is significantly offset leading to near equal combustion duration.

3. **Terminal phase:** The terminal phase response of the engine, at both part and full load operation is interesting considering that doubling of mixture H_2 fraction (from C1 to C4) also leads to doubling of the combustion duration, both in absolute degrees and fraction of full cycle terms. Towards addressing this response, some aspects pertaining to the thermal boundary layers and flame position in the vicinity of the position of peak pressure are reviewed.

Under typical SI engine like conditions, the boundary layer thickness is reported to be of the order of about a millimeter in the immediate vicinity of TDC for typical hydrocarbon fuels [97]. The boundary layer grows as per the equation (14).

$$\delta_T = 0.6(\alpha t)^{\frac{1}{2}} Re^{\frac{1}{5}} \tag{14}$$

It is evident from equation (14) that the boundary layer thickness grows as the square root of thermal diffusivity. Thus, with increasing H_2 fraction, the boundary layer thickness also increases and an increasing portion of mixture is present in the boundary layer. Considering the fact that higher H_2 fraction also entails enhanced convective losses (as discussed in Energy flow analysis and addressing the cooling load section) a greater fraction of mixture runs increasingly cooler as the mixture H_2 fraction increases. On the flame position in the vicinity of the position of peak pressure, simultaneous analysis of flame development (photographic) and in-cylinder pressure evolution suggests that the turbulent flame touches the wall farthest from the spark plug just after the position of peak pressure [21,91,98] and at this stage, another 20–25% of the mixture is yet to burn. This is also evident from simultaneous comparison of Figs. 9 and 10. The combustion of this 20–25% of the mixture constitutes the terminal phase. It is evident from the foregone discussion that with increasing mixture H_2 content, increasing fraction of relatively cooler mixture is burned in the terminal phase of combustion leading to an increase in the corresponding combustion duration. Based on the observations, the laminar flame propagation retard caused by the temperature drop is significant enough to overcome the laminar flame speed increase associated with higher mixture H_2 fractions (from C1 to C4). This is verified from the

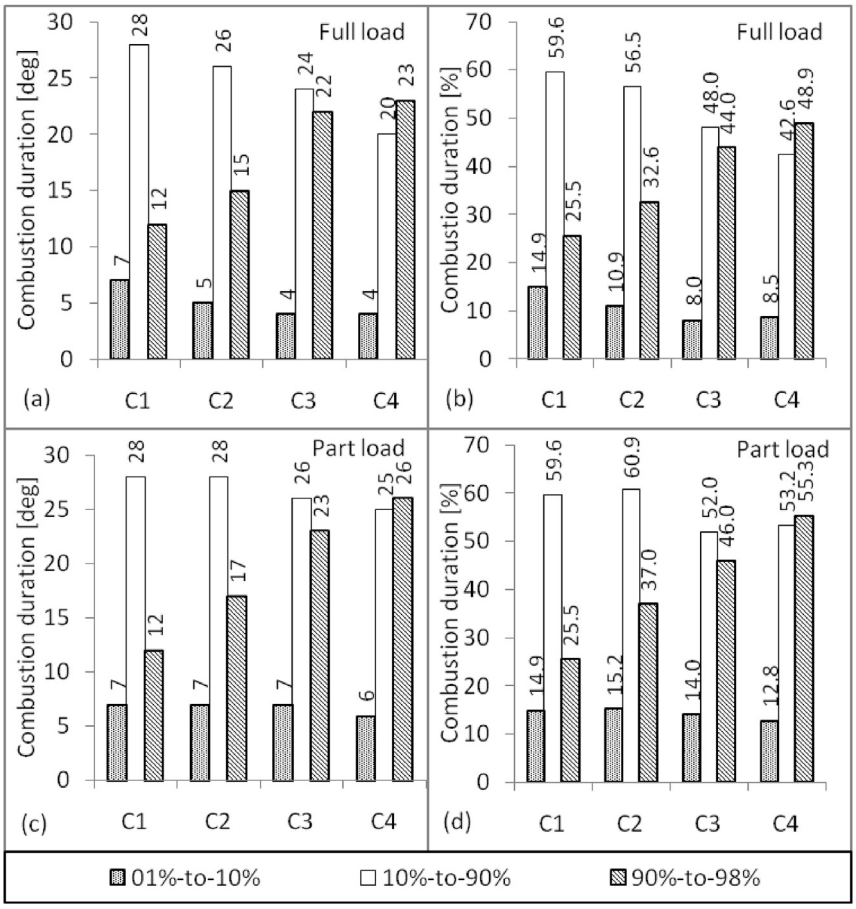

Fig. 11 – Combustion duration for full and part load operation.

1. **Initial development phase:** With an increase in the mixture H_2 fraction, the initial flame development period reduces for full load operation and remains broadly invariant for part load operation. This response can be addressed by analyzing the key factors that influence the flame development period like in-cylinder turbulence, mixture thermo-physical properties and the flame kernel energy balance [83–85]. Among the identified parameters, the reduction is primarily attributed to higher mixture reactivity and hence flame speed and more severe in-cylinder thermodynamic conditions (due to higher supported loads from C1 to C4). On the ignition energy front, with increasing H_2 fraction, the minimum ignition energy required will reduce as evident from the estimates based on equation (10) (in mJ; E_{min}:C1 ∝ 0.00337, E_{min}:C2 ∝ 0.00058, E_{min}:C3 ∝ 0.00031 and E_{min}:C4 ∝ 0.00011 refer [86]).

$$E_{min} \propto \rho C_p T \left(\frac{\alpha}{S_L}\right)^3 \tag{10}$$

comparison of laminar flame speed data for the four gas compositions as consolidated in Table 13.

It can be observed from Table 13 that for stoichiometric mixtures of gases C1 and C2, within a temperature difference of 100 K, the laminar flame speeds almost become equal while for C3 and C4, the laminar flame speed of C3 surpasses that of C4. This behavior is more pronounced at higher temperature as compared to lower temperatures. As for the sub-stoichiometric operation (relevant to the current study) while a 100 K increase causes the flame speed of C1 to just surpass that of C2, the flame speed of C3 significantly overshoots that of C4. Thus, it can be observed that temperature differences significantly counteract the influence of H_2 in the mixture, the required temperature difference being lower for leaner mixtures.

The foregone discussion clearly brings out the physics governing the nett heat release and pressure evolution in the engine cylinder as a function of syngas composition.

Table 13 – Laminar flame speed variation with temperature at stoichiometry.

	C1	C2	C3	C4	C1	C2	C3	C4
	Laminar flame speed (cm/s)							
	$\phi = 1.00$				$\phi = 0.85$			
400 K	27	52	63	93	23	42	52	75
450 K	37	68	83	120	31	57	68	99
500 K	48	88	106	152	42	73	90	126
550 K	64	113	135	191	56	97	116	162
600 K	83	144	172	236	74	124	149	204
650 K	108	185	215	292	97	159	189	256
700 K	140	230	268	359	127	204	–	319

Conclusions

The influence of key thermo-physical properties of H_2 containing gaseous mixture on an SI engine is addressed. A multi-pronged approach involving the analysis of mixture thermo-physical properties and flame structure based on established zero and one-dimensional chemical kinetics routines, thermodynamic engine simulation module and experimental investigations involving in-cylinder data acquisition is adopted. The results establish an increase in the engine cooling load with increasing Syngas H_2 fraction. The salient features of the investigation are summarized as below;

1. Preliminary thermodynamic and convective heat transfer analysis suggests direct influence of adiabatic flame temperature and convective heat transfer on the energy balance with laminar flame speed and flame quenching distance having a secondary influence.
2. The presence of H_2 in the mixture increases the adiabatic flame temperature and laminar flame speed attributed to a significant increase in temperature and radical (especially H and OH) gradient across the flame due to enhanced reaction rates.
3. The adiabatic flame temperature for the four syngas compositions considered is lower than the corresponding individual constituent flame temperature (attributed to diluents like CO_2 and N_2) and hence cannot be regarded as causative factors of higher convective heat flux.
4. Reduction of flame thickness and H specie domination results in lower than unity Lewis number. The two factors coupled with thermodynamic conditions (especially pressure) induce turbulence like influence on the flame propagation speed and potentially alter the engine thermo-kinematic response.
5. Peak load energy balance suggests an increase in the engine load with H_2 fraction. Over the entire range of composition, the cooling load is about 10 ± 3% higher than the typical higher hydrocarbon cooling load. While the higher cooling load is the consolidated influence of (identified) thermo-physical properties, the specific influence of thermal conductivity and diffusivity has been quantified using simulation studies.
6. As a consequence of increasing engine cooling load with H_2 fraction, the brake thermal efficiency that initially increases with H_2 fraction reduces at higher H_2 levels.
7. The general notion of post TDC combustion phasing being largely invariant for MBT operation, as established for conventional high hydrocarbon fuels, no longer holds for syngas fueled operation. The MBT operation position of peak pressure advances towards the TDC as the H_2 fraction in the syngas mixture increases, suggesting potential alteration of flame speed in the vicinity of TDC. While beyond the scope of the current investigation, the onset of flame instability and cellularity is suggested as a strong factor bringing about such a change.
8. Analysis of the heat release profile indicates a reduction in flame kernel development and fast burn phase duration with increase in the mixture H_2 fraction while the terminal phase duration increases.
9. The reduction of combustion duration for the first two phases of combustion is attributed to (a) reduced ignition energy requirement and (b) overall improvement in the mixture reactivity. The increase in the terminal phase of combustion is attributed to enhanced cooling (due to higher thermal conductivity/diffusivity) of the un-burned mixture, mostly in the boundary layer. The cooling effect is significant enough to overcome the flame propagation increase due to higher H_2 fraction.

REFERENCES

[1] White CM, Steeper RR, Lutz AE. The hydrogen-fueled internal combustion engine: a technical review. Int J Hydrogen Energy 2006;31(10):1292–305.
[2] Verhelst Sebastian, Wallner Thomas. Hydrogen-fueled internal combustion engines. Prog Energy Combust Sci 2009;35(6):490–527.
[3] Karim Ghazi A. Hydrogen as a spark ignition engine fuel. Int J Hydrogen Energy 2003;28(5):569–77.
[4] Hari Ganesh R, Subramanian V, Balasubramanian V, Mallikarjuna JM, Ramesh A, Sharma RP. Hydrogen fueled spark ignition engine with electronically controlled manifold injection: an experimental study. Renew Energy 2008;33(6):1324–33.
[5] Lee SJ, Yi HS, Kim ES. Combustion characteristics of intake port injection type hydrogen fueled engine. Int J Hydrogen Energy 1995;20(4):317–22.
[6] Liu Xing hua, Liu Fu shui, Zhou Lei, Sun Bai gang, Schock Harold J. Backfire prediction in a manifold injection hydrogen internal combustion engine. Int J Hydrogen Energy 2008;33(14):3847–55.
[7] Das LM. Hydrogen engine: research and development (r and d) programmes in Indian Institute of Technology (IIT), Delhi. Int J Hydrogen Energy 2002;27(9):953–65.
[8] Heffel James W. {NOx} emission and performance data for a hydrogen fueled internal combustion engine at 1500 rpm using exhaust gas recirculation. Int J Hydrogen Energy 2003;28(8):901–8.
[9] Ma Fanhua, Wang Yu, Liu Haiquan, Li Yong, Wang Junjun, Zhao Shuli. Experimental study on thermal efficiency and emission characteristics of a lean burn hydrogen enriched natural gas engine. Int J Hydrogen Energy 2007;32(18):5067–75.
[10] Allenby S, Chang WC, Megaritis A, Wyszyński ML. Hydrogen enrichment: a way to maintain combustion stability in a natural gas fuelled engine with exhaust gas recirculation, the

potential of fuel reforming. Proc Inst Mech Eng Part D J Automob Eng 2001;215(3):405–18.
[11] Ma Fanhua, Wang Yu. Study on the extension of lean operation limit through hydrogen enrichment in a natural gas spark-ignition engine. Int J Hydrogen Energy 2008;33(4):1416–24.
[12] Papagiannakis RG, Rakopoulos CD, Hountalas DT, Giakoumis EG. Study of the performance and exhaust emissions of a spark-ignited engine operating on syngas fuel. Int J Altern Propuls 2007;1(2):190–215.
[13] Boehman André L, Corre Olivier Le. Combustion of syngas in internal combustion engines. Combust Sci Technol 2008;180(6):1193–206.
[14] Baratieri M, Baggio P, Bosio B, Grigiante M, Longo GA. The use of biomass syngas in IC engines and CCGT plants: a comparative analysis. Appl Therm Eng 2009;29(16):3309–18.
[15] Martínez Juan Daniel, Mahkamov Khamid, Andrade Rubenildo V, Silva Lora Electo E. Syngas production in downdraft biomass gasifiers and its application using internal combustion engines. Renew Energy 2012;38(1):1–9.
[16] Karim GA, Wierzba I, Al-Alousi Y. Methane–hydrogen mixtures as fuels. Int J Hydrogen Energy 1996;21(7):625–31.
[17] Schefer RW. Hydrogen enrichment for improved lean flame stability. Int J Hydrogen Energy 2003;28(10):1131–41.
[18] Munshi SR, Nedelcu Costi, Harris Jonathan, Edwards Tommy, Williams J, Lynch Franklin, et al. Hydrogen blended natural gas operation of a heavy duty turbocharged lean burn spark ignition engine. Technical report, SAE Technical Paper. 2004.
[19] Bauer CG, Forest TW. Effect of hydrogen addition on the performance of methane-fueled vehicles. Part I: effect on SI engine performance. Int J Hydrogen Energy 2001;26(1):55–70.
[20] D'Andrea T, Henshaw PF, Ting DS-K. The addition of hydrogen to a gasoline-fuelled SI engine. Int J Hydrogen Energy 2004;29(14):1541–52.
[21] Heywood John B. Fundamentals of internal combustion engines. NY: McGraw Hill; 1988. p. 619.
[22] Nabi Md Nurun. Theoretical investigation of engine thermal efficiency, adiabatic flame temperature, NOx emission and combustion-related parameters for different oxygenated fuels. Appl Therm Eng 2010;30(8):839–44.
[23] Peters Norbert. Turbulent combustion. Cambridge University Press; 2000.
[24] Turns Stephen R. An introduction to combustion: concepts and applications. McGrw-Hill Companies, Inc; 2000.
[25] Dasappa S, Paul PJ, Mukunda HS, Rajan NKS, Sridhar G, Sridhar HV. Biomass gasification technology – a route to meet energy needs. Curr Sci 2004;87(7):908–16.
[26] Shivapuji Anand M, Dasappa S. Experiments and zero D modeling studies using specific Wiebe coefficients for producer gas as fuel in spark-ignited engines. Proc Inst Mech Eng Part C J Mech Eng Sci 2013;227(3):504–19.
[27] Shivapuji Anand M, Dasappa S. Selection and thermodynamic analysis of a turbocharger for a producer gas-fuelled multi-cylinder engine. Proc Inst Mech Eng Part A J Power Energy 2014;228(3):340–56.
[28] Shivapuji Anand M, Dasappa S. In-cylinder investigations and analysis of a SI gas engine fuelled with H_2 and CO rich syngas fuel: sensitivity analysis of combustion descriptors for engine diagnostics and control. Int J Hydrogen Energy 2014;39(28):15786–802.
[29] Sridhar G, Paul PJ, Mukunda HS. Biomass derived producer gas as a reciprocating engine fuel – an experimental analysis. Biomass Bioenergy 2001;21(1):61–72.
[30] Shivapuji AM, Dasappa S. Experimental studies on multi-cylinder natural gas engine fueled with producer gas. In: Proceedings of 19th European biomass conference and exhibition from research to industry and markets; 2011. p. 974–80.
[31] Shudo Toshio, Nakajima Yasuo, Futakuchi Takayuki. Thermal efficiency analysis in a hydrogen premixed combustion engine. JSAE Rev 2000;21(2):177–82.
[32] Shudo T, Nabetani S, Nakajima Y. Analysis of the degree of constant volume and cooling loss in a spark ignition engine fuelled with hydrogen. Int J Eng Res 2001;2(1):81–92.
[33] Shudo Toshio. Improving thermal efficiency by reducing cooling losses in hydrogen combustion engines. Int J Hydrogen Energy 2007;32(17):4285–93.
[34] Shudo Toshio, Suzuki Hiroyuki. Applicability of heat transfer equations to hydrogen combustion. JSAE Rev 2002;23(3):303–8.
[35] Demuynck Joachim, De Paepe Michel, Huisseune Henk, Sierens Roger, Vancoillie Jeroen, Verhelst Sebastian. On the applicability of empirical heat transfer models for hydrogen combustion engines. Int J Hydrogen Energy 2011;36(1):975–84.
[36] Knop Vincent, Benkenida Adlène, Jay Stéphane, Colin Olivier. Modelling of combustion and nitrogen oxide formation in hydrogen-fuelled internal combustion engines within a 3D CFD code. Int J Hydrogen Energy 2008;33(19):5083–97.
[37] Kee Robert J, Rupley Fran M, Miller James A. The chemkin thermodynamic data base, vol. 1; 1990.
[38] Dasappa S, Sridhar HV, Sridhar G, Paul PJ, Mukunda HS. Biomass gasification – a substitute to fossil fuel for heat application. Biomass Bioenergy 2003;25(6):637–49.
[39] Sandeep K, Dasappa S. Oxy-steam gasification of biomass for hydrogen rich syngas production using downdraft reactor configuration. Int J Energy Res 2014;38(2):174–88.
[40] Sandeep K, Dasappa S. First and second law thermodynamic analysis of air and oxy-steam biomass gasification. Int J Hydrogen Energy 2014;39(34):19474–84.
[41] Orhan Akansu S, Dulger Zafer, Kahraman Nafiz, Nejat Veziroglu T. Internal combustion engines fueled by natural gas–hydrogen mixtures. Int J Hydrogen Energy 2004;29(14):1527–39.
[42] Orhan Akansu S, Kahraman Nafiz, Ceper Bilge. Experimental study on a spark ignition engine fuelled by methane–hydrogen mixtures. Int J Hydrogen Energy 2007;32(17):4279–84.
[43] Dasappa S. On the estimation of power from a diesel engine converted for gas operation–a simple analysis. Power 2005;1:2.
[44] Wilke CR. A viscosity equation for gas mixtures. J Chem Phys 2004;18(4):517–9.
[45] Mathur S, Tondon PK, Saxena SC. Thermal conductivity of binary, ternary and quaternary mixtures of rare gases. Mol Phys 1967;12(6):569–79.
[46] Abraham John, Williams Forman A, Bracco Frediano V. A discussion of turbulent flame structure in premixed charges. Technical report, SAE Technical Paper. 1985.
[47] Kee Robert J, Rupley Fran M, Meeks Ellen, Miller James A, Chemkin III A. A fortran chemical kinetics package for the analysis of gas phase chemical and plasma kinetics. Sandia National Laboratories; 1996.
[48] Smith Gregory P, Golden David M, Frenklach Michael, Moriarty Nigel W, Eiteneer Boris, Goldenberg Mikhail, et al. Gri-mech 3.0. 1999.
[49] Law CK, Sung CJ. Structure, aerodynamics, and geometry of premixed flamelets. Prog Energy Combust Sci 2000;26(4):459–505.
[50] Lieuwen Tim, Yang Vigor, Yetter Richard. Synthesis gas combustion: fundamentals and applications. CRC Press; 2009.
[51] Glassman Irvin. Combustion. Academic Press; 1997.
[52] Im Hong G, Chen Jacqueline H. Preferential diffusion effects on the burning rate of interacting turbulent premixed hydrogen–air flames. Combust Flame 2002;131(3):246–58.

[53] Dinkelacker F, Manickam B, Muppala SPR. Modelling and simulation of lean premixed turbulent methane/hydrogen/air flames with an effective Lewis number approach. Combust Flame 2011;158(9):1742–9.
[54] Gelfand Boris E, Silnikov Mikhail V, Medvedev Sergey P, Khomik Sergey V. Thermo-Gas dynamics of hydrogen combustion and explosion. Springer; 2012.
[55] Liu Fengshan, Gülder Ömer L. Effects of H_2 and H preferential diffusion and unity Lewis number on superadiabatic flame temperatures in rich premixed methane flames. Combust Flame 2005;143(3):264–81.
[56] Kwon OC, Rozenchan G, Law CK. Cellular instabilities and self-acceleration of outwardly propagating spherical flames. Proceed Combust Inst 2002;29(2):1775–83.
[57] Li Hong-Meng, Li Guo-Xiu, Sun Zuo-Yu, Zhai Yue, Zhou Zi-Hang. Research on cellular instabilities of lean premixed syngas flames under various hydrogen fractions using a constant volume vessel. Energies 2014;7(7):4710–26.
[58] Moccia Vincenzo, D'Alessio Jacopo. Burning behaviour of high-pressure CH_4–H_2–air mixtures. Energies 2013;6(1):97–116.
[59] Bradley Derek, Sheppart CGW, Woolley R, Greenhalgh DA, Lockett RD. The development and structure of flame instabilities and cellularity at low Markstein numbers in explosions. Combust Flame 2000;122(1):195–209.
[60] Kitagawa Toshiaki, Nakahara Takashi, Maruyama Kosuke, Kado Kunihiro, Hayakawa Akihiro, Kobayashi Shoichi. Turbulent burning velocity of hydrogen–air premixed propagating flames at elevated pressures. Int J Hydrogen Energy 2008;33(20):5842–9.
[61] Jomaas Grunde, Law CK, Bechtold JK. On transition to cellularity in expanding spherical flames. J Fluid Mech 2007;583:1–26.
[62] Frassoldati A, Faravelli T, Ranzi E. The ignition, combustion and flame structure of carbon monoxide/hydrogen mixtures. Note 1: detailed kinetic modeling of syngas combustion also in presence of nitrogen compounds. Int J Hydrogen Energy 2007;32(15):3471–85.
[63] Cuoci A, Frassoldati A, Buzzi Ferraris G, Faravelli T, Ranzi E. The ignition, combustion and flame structure of carbon monoxide/hydrogen mixtures. note 2: fluid dynamics and kinetic aspects of syngas combustion. Int J Hydrogen Energy 2007;32(15):3486–500.
[64] Burbano Hugo J, Pareja Jhon, Amell Andrés A. Laminar burning velocities and flame stability analysis of H_2/CO/air mixtures with dilution of N_2 and CO_2. Int J Hydrogen Energy 2011;36(4):3232–42.
[65] Pipitone Emiliano. A comparison between combustion phase indicators for optimal spark timing. J Eng Gas Turb Power 2008;130(5):052808.
[66] Dasappa S, Sridhar G, Paul PJ. Adaptation of small capacity natural gas engine for producer gas operation. Proceed Inst Mech Eng Part C J Mech Eng Sci 2011. http://dx.doi.org/10.1177/0954406211424678.
[67] Kutlar Osman Akin, Arslan Hikmet, Calik Alper Tolga. Methods to improve efficiency of four stroke, spark ignition engines at part load. Energy Convers Manag 2005;46(20):3202–20.
[68] Schäfer Fred, Van Basshuysen Richard. Reduced emissions and fuel consumption in automobile engines. Springer; 1995.
[69] Yüksel F, Ceviz MA. Thermal balance of a four stroke SI engine operating on hydrogen as a supplementary fuel. Energy 2003;28(11):1069–80.
[70] Wallace Scott J, Kremer Gregory G. Diesel engine energy balance study operating on diesel and biodiesel fuels. In: ASME 2008 International mechanical engineering congress and exposition. American Society of Mechanical Engineers; 2008. p. 337–43.
[71] Annand WJD. Heat transfer in the cylinders of reciprocating internal combustion engines. Proceed Inst Mech Eng 1963;177(1):973–96.
[72] Borman Gary, Nishiwaki Kazuie. Internal-combustion engine heat transfer. Prog Energy Combust Sci 1987;13(1):1–46.
[73] Incropera Frank P. Introduction to heat transfer. John Wiley & Sons; 2011.
[74] Ismail Saleel, Mehta Pramod S. Second law analysis of hydrogen–air combustion in a spark ignition engine. Int J Hydrogen Energy 2011;36(1):931–46.
[75] Kouremenos DA, Rakopoulos CD, Hountalas DT, Zannis TK. Development of a detailed friction model to predict mechanical losses at elevated maximum combustion pressures. Technical report, SAE Technical Paper. 2001.
[76] Sandoval Daniel, Heywood John B. An improved friction model for spark-ignition engines. Technical report, SAE Technical paper. 2003.
[77] Hubbard M, Dobson PD, Powell JD. Closed loop control of spark advance using a cylinder pressure sensor. J Dyn Syst Meas Control 1976;98:414.
[78] Beccari A, Pipitone E. Proportional integral spark timing control by means of in-cylinder pressure analysis. In: FISITA 2004 World Automotive Congress; 2004.
[79] Shayler PJ, Wiseman MW, Ma T. Improving the determination of mass fraction burnt. 1990. Technical report, SAE Technical Paper.
[80] Brunt Michael FJ, Emtage Andrew L. Evaluation of burn rate routines and analysis errors. Technical report, SAE Technical Paper. 1997.
[81] Brunt Michael FJ, Rai Harjit, Emtage Andrew L. The calculation of heat release energy from engine cylinder pressure data. Technical report, SAE Technical Paper. 1998.
[82] Baratta Mirko, d'Ambrosio Stefano, Spessa Ezio, Vassallo Alberto. Cycle-resolved detection of combustion start in SI engines by means of different in-cylinder pressure data reduction techniques. In: ASME 2006 internal combustion engine division spring technical conference. American Society of Mechanical Engineers; 2006. p. 303–16.
[83] Pischinger Stefan, Heywood John B. A model for flame kernel development in a spark-ignition engine. In: Symposium (International) on Combustion, vol. 23. Elsevier; 1991. p. 1033–40.
[84] Shen Huixian, Hinze Peter C, Heywood John B. A model for flame initiation and early development in SI engine and its application to cycle-to-cycle variations. Technical report, SAE Technical Paper. 1994.
[85] Eisazadeh-Far Kian, Parsinejad Farzan, Metghalchi Hameed, Keck James C. On flame kernel formation and propagation in premixed gases. Combust Flame 2010;157(12):2211–21.
[86] Kurdyumov V, Blasco J, Sánchez AL, Linan A. On the calculation of the minimum ignition energy. Combust Flame 2004;136(3):394–7.
[87] Maly Rudolf. Spark ignition: its physics and effect on the internal combustion engine. In: Fuel economy. Springer; 1984. p. 91–148.
[88] Cho Hanseong, Lee Kwiyoung, Lee Jonghwa, Yoo Jaisuk, Min Kyoungdoug. Measurements and modeling of residual gas fraction in SI engines. Technical report, SAE Technical Paper. 2001.
[89] Giansetti Pascal, Colin Guillaume, Higelin Pascal, Chamaillard Yann. Residual gas fraction measurement and computation. Int J Eng Res 2007;8(4):347–64.
[90] Gatowski Jan A, Heywood John B, Deleplace Christian. Flame photographs in a spark-ignition engine. Combust Flame 1984;56(1):71–81.

[91] Keck James C. Turbulent flame structure and speed in spark-ignition engines. In: Symposium (International) on Combustion, vol. 19. Elsevier; 1982. p. 1451–66.
[92] Mounaïm-Rousselle Christine, Landry Ludovic, Halter Fabien, Foucher Fabrice. Experimental characteristics of turbulent premixed flame in a boosted spark-ignition engine. Proceed Combust Inst 2013;34(2):2941–9.
[93] Peters N. Length and time scales in turbulent combustion. In: Turbulent reactive flows. Springer; 1989. p. 242–56.
[94] Peters N. The turbulent burning velocity for large-scale and small-scale turbulence. J Fluid Mech 1999;384:107–32.
[95] Borghi R. On the structure and morphology of turbulent premixed flames. In: Recent advances in the aerospace sciences. Springer; 1985. p. 117–38.
[96] Pope SB. Turbulent premixed flames. Ann Rev Fluid Mech 1987;19(1):237–70.
[97] Lyford-Pike Edward J, Heywood John B. Thermal boundary layer thickness in the cylinder of a spark-ignition engine. Int J Heat Mass Transfer 1984;27(10):1873–8.
[98] Beretta GP, Rashidi M, Keck JC. Turbulent flame propagation and combustion in spark ignition engines. Combust Flame 1983;52:217–45.